Handbook of PHYSICS in MEDICINE and BIOLOGY

Edited by

Robert Splinter

CRC Press
Taylor & Francis Group

Handbook of PHYSICS in MEDICINE and BIOLOGY

Handbook of PHYSICS in MEDICINE and BIOLOGY

Edited by

Robert Splinter

CRC Press
Taylor & Francis Group
Boca Raton London New York

CRC Press is an imprint of the
Taylor & Francis Group, an **informa** business

CRC Press
Taylor & Francis Group
6000 Broken Sound Parkway NW, Suite 300
Boca Raton, FL 33487-2742

Version Date: 20140512

International Standard Book Number-13: 978-1-4200-7525-0 (eBook - PDF)

Visit the Taylor & Francis Web site at
http://www.taylorandfrancis.com

and the CRC Press Web site at
http://www.crcpress.com

To my dad Hans, for supporting my goals and believing in my potential.

Contents

Section III Biomechanics

Section IV Bioelectrical Physics

Section V Diagnostic Physics

Section VI Physics of Accessory Medicine

Section VII Physics of Bioengineering

Preface

Biology: The New Physics

The focus of this book is the use of physics and physical chemistry in biological organisms, in addition to the physical aspects of the tools used to investigate biological organisms. The term physics is used in the broadest sense of the word, extending to fluid dynamics, mechanics, and electronics. This book provides the physical and technological foundation for understanding biological functioning in general, as well as offering technical and theoretical support for biomedical research.

A frequently cited phrase coined for the new millennium is that biology is the new physics. This concept holds true in bioengineering and diagnostic tool development as well as in general biological research. Both biology and medicine have had a close collaboration with physics over centuries, at both the basic and applied levels. Major new developments in biology are motivated by broad aspects of physics, including electronics and mechanics. In addition to physicists developing instruments for biologists to perform research and create methods to analyze and reproduce biological archetypes, biologists are more and more likely to be the creative minds behind biomedical physics concept development. This book covers the engineering and physics that can help explain clinical conditions and also describes the technology used to examine clinical conditions. In addition, it discusses emerging technologies that will advance the role of medicine and assist in improving diagnostic and therapeutic medical applications.

About the Book

Handbook of Physics in Medicine and Biology is designed as a reference manual for professionals and students in the biomedical profession. It is also a resource on the technological aspects of the broad range of scientific topics for biomedical physics taught in a university setting. The book provides an introduction to engineering technology as applied to biological systems. The scientific background offered will aid in the evaluation and design of devices and techniques that can be used to acquire pertinent clinical information and develop an understanding of pertinent biological processes that will assist in the general understanding of how biology works and how biological entities function.

Each chapter contains references for additional information on specific topics that cannot be discussed in detail due to the focus of the book or based on the exhaustive background available in that particular field.

The goal of this work is to provide a professionally relevant handbook to further the education for students and professionals in biology, medicine, and biomedical physics. The material offers the fundamental knowledge and skill sets required for anyone pursuing a career in the medical and biomedical field. In this book, the reader is given an opportunity to learn about the rapidly developing and innovative techniques for understanding biological processes from an engineering perspective, as well as the science behind diagnostic methods and imaging techniques. Ultimately, we seek to improve our understanding of diseases and our ability to treat them.

Interdisciplinary Treatment

The interaction of physics and living or biological systems starts at the cellular and molecular levels, extending to the description of the operation of the organism in addition to the diagnostic methods of identifying potential problems or gaining a detailed understanding of the operation of the organism. Biomedical physics is often described as biomedical engineering, in contrast to biotechnology, which addresses the biochemistry. All aspects of diagnostic and therapeutic modalities are treated in their relation to normal physiological functions.

The use of physics in medicine and biology will assist in increasing an understanding of the molecular and cellular principles that create the macro diagnostic values measured on the outside with current diagnostic and physical devices.

The objectives of the book are to provide an insight into the elementary laws of physics and the roles they play in the biological organism, in addition to the application of the basic laws of physics applied to the measurement of biological phenomena and the interpretation of these data. Additionally, the authors describe the biological operation by means of physics theory wherever applicable. The various aspects of physics involved in biology are the following: thermodynamics: cellular metabolism; energy: conservation of energy in biological processes; electricity: cellular depolarization; kinetics/mechanics: muscle contraction and skeletal motion, and waves and sound;

radiation: vision; and last but not least fluid dynamics: breathing and blood flow.

Furthermore, the chapters discuss in detail the physics involved in developing biologically alternative detection and signal processing techniques.

Organization

The organization of this text follows the hierarchy of the physical description of the operation of biological building blocks (cells and organs) to the functioning of various organs. The biological function is described at the electric, mechanical, electromagnetic, thermodynamic, and hydrodynamic levels for the respective metric and nonmetric characteristics of the organs. Following the physical description of the biological constituents, the book addresses the principles of a range of clinical diagnostic methods. It also looks at the technological aspects of specific therapeutic applications.

Brief Description of the Chapters

The book begins with a basic background description of specific biological features and delves into the physics of explicit anatomical structures such as the basic building block: the cell. Cellular metabolism is analyzed in terms of cellular thermodynamics, with the ionic mechanism for the transmembrane potential, after which the book describes the concepts of specific sensory functions. Next, the chapters explain more specific biological functions from a physics perspective—starting with electrophysiology, followed by fluid dynamics for blood and air function. After the biological description, the book outlines certain analytical modalities such as imaging and supporting diagnostic methods. A final section turns to future perspectives related to the new field of tissue engineering, including the biophysics of prostheses and the physics concepts in regenerative medicine.

The outline of the book has the following basic structure.

Section I of the book is a detailed description of atomic, molecular, and cellular biological physics. Chapters 1 through 5 describe cellular activity, including action potential generation and conduction.

Section II describes the physics of perception as well as sensory alternatives based on biology developed with physics principles. Chapters 6 through 11 cover the basic senses as well as additional means of perception and arriving at a diagnostic conclusion.

Section III focuses on the mechanics in biology. Chapters 12 through 19 give a detailed description of the mechanical engineering of motion, and liquid and gas fluid dynamics.

Section IV is an overview of the electrical engineering aspects of medical device design and electrical events in biology. Chapters 20 and 21 delve into electrode design and electrical detection, respectively.

Section V is the diagnostic portion of the book describing imaging techniques and alternate diagnostic methods. Chapters 22 through 40 give the scientific background of several conventional imaging methods and the mechanism of action on which their operation is based, in addition to several novel and upcoming sensing and imaging techniques.

Section VI describes some affiliate biology and physics, with a brief review of the science behind nuclear medicine and some engineering aspects of upcoming diagnostic methods. Chapters 41 through 43 introduce some new technology as well as state-of-the-art technology that has its own place in medicine and biology.

Section VII is the conclusion that delves into the physics behind regenerative medicine aspects in Chapter 44.

Audience

This book targets medical professionals and students involved in physical anthropology, forensic pathology, medical practice, medical device development, and diagnostic design. It is also appropriate for graduate level education in (bio)medical physics as well as in biomedical engineering and related disciplines.

Related Textbooks

1. Cameron JR, Skofronick JG, and Grant RM, *Physics of the Body*, 2nd edition, Medical Physics Publishing, Madison, WI, 1999.
2. Kane SA, *Introduction to Physics in Modern Medicine*, Taylor & Francis Publishing, London, 2003.
3. Davidovits P, *Physics in Biology and Medicine*, 3rd edition, Academic Press, Burlington, MA, 2008.
4. Tuszynski JA and Dixon JM, *Biomedical Applications of Introductory Physics*, John Wiley and Sons, New York, NY, 2001.

Acknowledgments

The authors acknowledge the contributions from various authors as well as the inspiration and contributions provided by students and professionals in the various fields of biophysical sciences. The detailed critique by each respective individual significantly enhanced the value of the biological, physical, and mathematical contents of this book.

The authors also acknowledge the assistance by both illustrative and theoretical means from all hospitals and industry, and the numerous individuals who are not mentioned individually but are nonetheless equally valuable for sharing their biomedical and physics information and illustrations with the reader and the authors, respectively. Great care has been taken to ensure that the source for each illustration is provided and to acknowledge the contributions of all institutions and individuals with proper tribute.

Editor

Robert Splinter received his master's degree from the Eindhoven University of Technology, Eindhoven, the Netherlands and his doctoral degree from the VU University of Amsterdam, Amsterdam, the Netherlands. He has worked in biomedical engineering for over 20 years, both in a clinical setting and in medical device development. He has been affiliated with the physics department of the University of North Carolina at Charlotte for over 20 years as an adjunct professor and was a core team member for the establishment of the interdisciplinary biology graduate program at UNCC. In addition, he served on the graduate boards of the University of Alabama at Birmingham, Birmingham, Alabama and the University of Tennessee Space Institute, Tulahoma, Tennessee. Dr. Splinter has cofounded several biomedical startup companies and served as technology manager in various capacities. He is the co-owner of several US and international patents and patent applications on methodologies using applied physics in the biomedical field. He has published more than 100 peer-reviewed papers in international journals and conference proceedings, as well as several books.

Contributors

Jean-Marc Aimonetti
Laboratory of Integrative and Adaptative Neurobiology
CNRS—Université de Provence
Aix-Marseille Université, Marseille, France

Beth J. Allison
Department of Physiology
Monash University
Victoria, Australia

David Baldwin
University of Western Australia
Perth, Western Australia, Australia

Manish Bothara
Portland State University
Portland, Oregon

Sonja Braun-Sand
Department of Chemistry
University of Colorado at Colorado Springs
Colorado Springs, Colorado

Hélio Chiarini-Garcia
Department of Morphology
Federal University of Minas Gerais
Belo Horizonte, Minas Gerais, Brazil

Ravishankar Chityala
SDVL
Minneapolis, Minnesota

David T. Corr
Rensselaer Polytechnic Institute
Troy, New York

Kevin A. Croussore
Fujitsu Laboratories of America
Fujitsu Network Communications
Richardson, Texas

Ryan C.N. D'Arcy
Institute for Biodiagnostics (Atlantic)
National Research Council Canada
Dalhousie University
Halifax, Nova Scotia, Canada

Mari Dezawa
Department of Stem Cell Biology and Histology
Tohoku University
Aoba-ku, Sendai, Japan

Didier Dréau
Department of Biology
University of North Carolina at Charlotte
Charlotte, North Carolina

Kert Edward
Department of Physics and Optical Sciences
University of North Carolina at Charlotte
Charlotte, North Carolina

Paul Elliot
Tessera, Inc.
Charlotte, North Carolina

Martin F. Finlan
Physical Sciences Consultant
Doncaster, United Kingdom

Gábor Fülöp
Heart Center
Semmelweis University
Budapest, Hungary

Paola Garcia
University of Colorado at Colorado Springs
Colorado Springs, Colorado

Jodie R. Gawryluk
Institute for Biodiagnostics (Atlantic)
National Research Council and Neuroscience Institute
Dalhousie University
Halifax, Nova Scotia, Canada

Cynthia Gibas
Department of Bioinformatics and Genomics
University of North Carolina at Charlotte
Charlotte, North Carolina

Frank Gijsen
Department of Biomedical Engineering
Biomechanics Laboratory
Rotterdam, the Netherlands

Mark S. Hedrick
Department of Audiology and Speech Pathology
The University of Tennessee
Knoxville, Tennessee

Myriam C. Herrera
Departamento de Biongeniería
Universidad Nacional de Tucumán and Instituto Superior de Investigaciones Biológicas
Tucumán, Argentina

El-Sayed H. Ibrahim
Department of Radiology
University of Florida
Jacksonville, Florida

Naohiro Ikeda
Department of Ophthalmology
Hyogo College of Medicine
Nishinomiya, Hyogo, Japan

Tomohiro Ikeda
Department of Ophthalmology
Hyogo College of Medicine
Nishinomiya, Hyogo, Japan

Hiroto Ishikawa
Department of Ophthalmology
Hyogo College of Medicine
Nishinomiya, Hyogo, Japan

Takuji Ishikawa
Department of Bioengineering and Robotics
Tohoku University
Aoba-ku, Sendai, Japan

Sanae Kanno
Department of Ophthalmology
Hyogo College of Medicine
Nishinomiya, Hyogo, Japan

Orsolya Kiss
Semmelweis University Heart Center
Semmelweis University of Medicine
Budapest, Hungary

Vindhya Kunduru
Department of Electrical and Computer Engineering
Portland State University
Portland, Oregon

Amanda W. Lund
Rensselaer Polytechnic Institute
Troy, New York

Rossana E. Madrid
Departamento de Biongeniería
Universidad Nacional de Tucumán and Instituto Superior de Investigaciones Biológicas
Tucumán, Argentina

Michael Markl
Department of Diagnostic Radiology, Medical Physics
University of Hospital Freiburg
Freiburg, Germany

Carmen C. Mayorga Martinez
Departamento de Biongeniería
Universidad Nacional de Tucumán and Instituto Superior de Investigaciones Biológicas
Tucumán, Argentina

Pál Maurovich-Horvat
Massachusetts General Hospital
Harvard Medical School
Boston, Massachusetts

Rossana Correa Netto Melo
Department of Biology
Federal University of Juiz de Fora
Juiz de Fora, Minas Gerais, Brazil

Juan Jiménez Millán
Departamento de Geología
Universidad de Jaén
Jaén, Spain

Osamu Mimura
Department of Biology
Hyogo College of Medicine
Nishinomiya, Hyogo, Japan

Timothy Moss
Department of Physiology
Monash University
Victoria, Australia

Sriram Muthukumar
Intel Corporation
Chandler, Arizona

Fernando Nieto
Departamento de Mineralogía y Petrología
Granada, Spain

Dmitriv V. Nikolaev
Scientific Research Centre "MEDASS"
Moscow, Russia

John A. Notte
Director of Research and Development
Carl Zeiss SMT, Inc.
Peabody, Massachusetts

Nael F. Osman
Johns Hopkins University
Baltimore, Maryland

István Osztheimer
Semmelweis University of Medicine
Budapest, Hungary

Gregory M. Palmer
Department of Radiation Oncology
Duke University
Durham, North Carolina

Christian Parigger
The Center for Laser Applications
University of Tennessee Space Institute, University of Tennessee
Tullahoma, Tennessee

Gleydes Gambogi Parreira
Department of Morphology
Federal University of Minas Gerais
Belo Horizonte, Minas Gerais, Brazil

John Pearce
Department of Electrical and Computer Engineering
University of Texas at Austin
Austin, Texas

Daniel S. Pickard
Department of Electrical Engineering
National University of Singapore
Singapore

Pavlina Pike
Department of Radiology
University of Alabama at Birmingham
Birmingham, Alabama

Jane Pillow
School of Women's and Infants' Health
University of Western Australia
Women's and Newborns' Health Service
Perth, Western Australia, Australia

George E. Plopper
Rensselaer Polytechnic Institute
Troy, New York

Shalini Prasad
Department of Electrical Engineering
Arizona State University
Tempe, Arizona

Sasa Radovanovic
Laboratory for Neurophysiology
Institute for Medical Research
Belgrade, Serbia

Sergey G. Rudnev
Institute of Numerical Mathematics
Russian Academy of Sciences
Moscow, Russia

Alexander V. Smirnov
Scientific Research Centre "MEDASS"
Moscow, Russia

Robert Splinter
Department of Physics and Optical Sciences
University of North Carolina at Charlotte
Charlotte, North Carolina

Aurélien F. Stalder
Department of Diagnostic Radiology, Medical Physics
University of Hospital Freiburg
Freiburg, Germany

Ernesto F. Treo
Departamento de Biongeniería
Universidad Nacional de Tucumán and Instituto Superior de Investigaciones Biológicas
Tucumán, Argentina

Rudolf Verdaasdonk
Physics and Medical Technology
VU University Amsterdam
Amsterdam, the Netherlands

Karthik Vishwanath
Department of Biomedical Engineering
Duke University
Durham, North Carolina

Juha Voipio
Department of Biosciences
University of Helsinki
Helsinki, Finland

Shelley J. Wilkins
Department of Physical and Theoretical Chemistry
Oxford University
Oxford, United Kingdom
and
Orbital Instruments Ltd
Doncaster, United Kingdom

Thomas Wolkow
Department of Biology
University of Colorado at Colorado Springs
Colorado Springs, Colorado

Yamini Yadav
Department of Electrical and Computer Engineering
Portland State University
Portland, Oregon

I

Anatomical Physics

1

Physics of the Cell Membrane

Thomas Wolkow

1.1 Introduction

The plasma membrane and those of intracellular organelles are composed of lipids and proteins arranged in a dynamic lipid bilayer. The structures and mechanical features of both components are described herein.

1.2 Cellular Membranes are Elastic Solids

The integrity of cellular membranes is routinely challenged by external and internal forces.[1] External forces include high-frequency vibrations, fluid shear stress, and osmotic and gravitational pressure gradients. Internal forces include hydrostatic pressure as well as those produced by cytoskeletal cables that push outward to orchestrate cellular movements, morphological changes, growth, and adhesion.

The physical characteristics of membranes that allow them to withstand such forces have been described by measuring membrane parameters before and after force is applied.[1] Researchers tend to employ human red blood cells (RBCs) and techniques like micropipette aspiration and patch–clamp devices to obtain these measurements. Overall, their results demonstrate that biological membranes respond like elastic solids when mechanical operations are used to compress, expand, bend, and extend a defined membrane area.

Within a drop of fluid that is not surrounded by a cellular membrane, the relationship between surface tension and pressure is described by the law of Laplace. Given a uniform surface tension (σ), internal pressure (P), and radius (R) of the drop, the law states that

$$P = \frac{2\sigma}{R}. \tag{1.1}$$

When modeling this relationship in a cell, one might think that the density of the membrane reacts to pressure differences between the external and internal environments. However, density, which describes the compressibility of lipids within the bilayer, remains constant under physiologically relevant pressures (100 atm).[1] Surface area displays somewhat weaker resistance and does undergo some change, but only 2–4% before rupturing. The tensile force (F_t) on the membrane is expressed in Equation 1.2 for this situation:

$$F_t = K_A \frac{\Delta A}{A_0}, \tag{1.2}$$

where ΔA is the increase in bilayer surface area from the original area A_0, K_A is the area expansion constant (between 10^2 and 10^3 mN/m), and F_t is tension (between 3 and 30 mN/m). And while surface area expands, membrane thickness changes proportionally so that

$$\frac{\Delta A}{A_0} = \frac{\Delta h}{h_0}, \tag{1.3}$$

where h_0 represents original membrane thickness. But the membrane response to shear stress is what clearly describes it as an elastic solid. Using two silica beads and optical traps to exert shear stress across an RBC[2] (Figure 1.1), elasticity can be seen

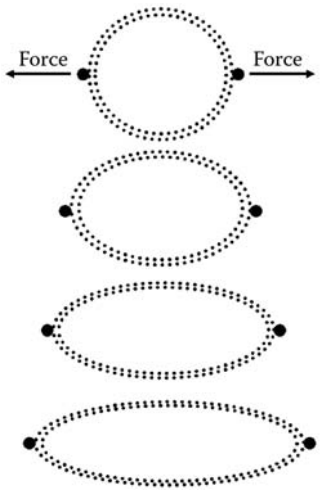

FIGURE 1.1 Membrane response to shear stress has been measured using optical traps and silica beads (black ovals) to apply force across RBCs.[2]

as this membrane elongates in the direction of applied force F. It can be shown that the diameter of the RBC obeys Equation 1.4:

$$D = D_0 - \frac{F}{2\pi\mu}, \tag{1.4}$$

where D is the diameter of the RBC, D_0 is the original diameter, and μ is the shear stress applied by the optical trap.

Importantly, this elastic behavior seems to be almost completely dependent upon a flexible network of cytoskeletal elements beneath the membrane surface.[3,4] Thus it is the underlying cytoskeleton that allows membranes to bend, flex, and resist rupture under physiologically stressful conditions.

1.3 Lipids

The major constituents of biological membranes are lipids, which are amphipathic molecules composed of a hydrophobic fatty acid chain and a hydrophilic head group (Figure 1.2).

Fatty acids are hydrocarbon chains (typically 16–18 carbons long) containing a terminal carboxyl group, and are synthesized in the cytoplasm from acetyl-CoA molecules produced in mitochondria. Fatty acids include saturated forms (e.g., palmitate and stearate) wherein carbon atoms are bonded with a maximum number of hydrogens, and the more common unsaturated forms (e.g., oleate) containing at least one kink-inducing double bond. When in excess, free fatty acids are transported to the space between the leaflets of the endoplasmic reticulum (ER) and the Golgi, where they are transformed into triacylglycerols or cholesteryl esters and stockpiled within membrane-bound organelles called lipid droplets.[5] These lipids will later be used for purposes of adenosine triphosphate (ATP) production, membrane synthesis, and steroid synthesis. For example, lipids contained within droplets and modified with a polar head group containing phosphate, ethanolamine, choline, serine, inositol, or sphingomyelin are used to synthesize the structural lipids of cellular membranes.

Structural lipids are members of the glycerophospholipid and sphingolipid families.[6] Sphingolipids have a ceramide head group built from an amino acid backbone and longer hydrocarbon chains that are predominantly unsaturated. These unsaturated chains allow sphingolipids to pack together closely and form a more solid gel phase within the liquid-disordered glycerophospholipid environment. Cholesterol commonly exists in sphingolipid domains and causes them to transform into a liquid-ordered phase wherein lipids are tightly packed with freedom to diffuse laterally. These liquid-ordered phases or lipid rafts[7] exist only in the outer membrane leaflet and are connected to uncharacterized domains of the inner leaflet.[8] Within lipid rafts, specific sets of membrane-associated proteins are assembled, which promote interactions among specific groups of proteins and inhibit cross talk with others.[9]

Microdomains, such as lipid rafts, can affect the curvature and thus the energy (E_{sphere}) of biological membranes[10] (Figure 1.3). For a membrane without spontaneous curvature, the energy of the membrane is given by

$$E_{sphere} = \gamma S + 8\pi\kappa, \tag{1.5}$$

where γ is surface tension, S is membrane area, and $\kappa = 20K_BT$ is bending rigidity; the thermal energy scale at room temperature is $K_BT = 4 \times 10^{-21}$ J. Microdomains that induce small invaginations increase the membrane energy by approximately $8\pi\kappa$. Atomic force microscopy (AFM) measurements suggest that these microdomains are stiff, as their elasticity moduli may be approximately 30% higher than the surrounding membrane area.[11]

1.3.1 Membrane-Associated Proteins

Proteins are gene products that can be distinguished based on location, function, and chemical composition. Two principal types of proteins exist within the membrane environment.

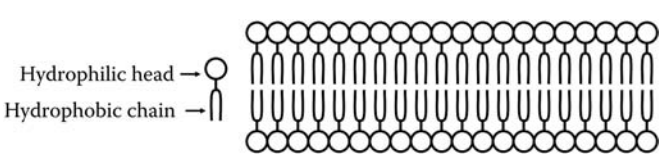

FIGURE 1.2 Lipids are major constituents of biological membranes.

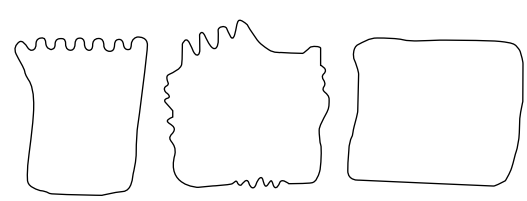

FIGURE 1.3 Cell curvature is a function of structural lipid composition.

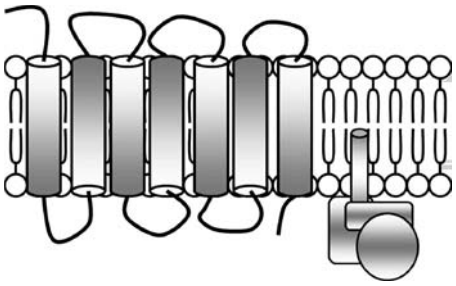

FIGURE 1.4 Transmembrane proteins (left) and peripheral proteins (right) populate biological membranes.

Transmembrane (or intrinsic) proteins cross the bilayer and may function as cellular receptors required for cell-to-cell communication and adhesion, or as transporters that shuttle various particles (including ions, glucose, and proteins) across the membrane. Peripheral (or extrinsic) proteins associate with the internal or external layer of the membrane where they may affect cell shape (BAR domain proteins), or possibly facilitate receptor-dependent signaling pathways (Figure 1.4). Two other groups of proteins (glycoproteins and lipoproteins) are also discussed because of their broad influence on membranes and lipid homeostasis.

1.3.2 Transmembrane Proteins

All transmembrane proteins contain membrane-spanning domains composed primarily of nonpolar residues assembled into secondary structures that neutralize the polarity of peptide bond elements. These membrane-spanning domains typically assume flexible α-helical or rigid β-sheet secondary structures. Ligand binding seems to stimulate downstream receptor signaling events by altering the electrostatic field of the receptor and/or eliciting changes in receptor conformation. Currently, the technology to record measurements of single receptors at the surface of living cells is absent. However, AFM studies of the α-amino-3-hydroxy-5-methylisoxazole-4-propionic acid-type glutamate receptors (AMPAR) demonstrate that upon ligand binding, the elastic modulus of the receptor nanodomains permanently decreases by 20–30% relative to the surrounding membrane area.[12] This probably occurs because activated receptors are sometimes internalized and removed from the cell surface by the endocytotic pathways discussed below.

1.3.3 Peripheral Proteins

Peripheral proteins may associate with membranes through physical interactions with transmembrane proteins or because of post-translational modifications. These modifications result in the addition of a hydrophobic fatty acid, such as palmitate, or a hydrophobic glycolipid group. Glycolipid modifications include glycosylphosphatidylinositol (GPI) modifications that contain two fatty acid chains, an inositol in addition to other sugars, and ethanolamine. By nature of their hydrophobicities, these fatty acid and GPI groups become inserted into the bilayer and thereby serve to anchor the protein to the membrane.

1.3.4 Glycoproteins

Glycoproteins are carbohydrate-modified proteins. These carbohydrate groups not only assist in protein folding, stability, and aggregation, but when present on transmembrane proteins may affect cell–cell adhesion via electrostatic, hydrophobic, and covalent interactions. Adhesion forces can also result from surface tension that arises in the fluid interface formed with glycoprotein-decorated cellular surfaces. For example, glycoprotein-decorated stigmas and lipoprotein-decorated pollen grains interact with an adhesion force of approximately 2×10^{-8} N due to surface tension and a fluid interface.[13] Four types of glycosylations are known: GPI anchors, C-glycosylation, *N*-glycosylation, and *O*-glycosylation. As discussed above, GPI anchors contain sugar moieties that participate in the production of peripheral proteins.

C-glycoproteins are produced when sugars are directly linked to the protein by carbon–carbon bonds, hence the name C-glycoprotein.[14,15] To date, C-mannosylation of human RNase 2 is the most well-characterized example of C-glycosylation. It occurs on the first Try residue in the Trp–X–X–Trp motif of RNase 2 and influences the specific orientation of the modified Trp in the tertiary structure.

N-glycosylation occurs in the ER and begins when a 14-sugar precursor containing three glucose, nine mannose, and two *N*-acetylglucosamine molecules is transferred to an asparagine (N) residue in one of the following tripeptide motifs, Asn–X–Ser, Asn–X–Thr, or Asn–X–Cys.[14] This precursor complex is then modified to produce mature *N*-glycosylation patterns that contain, for example, more mannose or different types of saccharides or more than two *N*-acetylglucosamines.

O-glycosylation occurs in both the ER and the Golgi as glycosyl transferases modify the OH group of amino acids like serine or threonine with one sugar at a time, typically beginning with *N*-acetylgalactosamine.[14] To date, roughly 100 *O*-glycosylated proteins are known.[16]

1.3.5 Lipoproteins

Lipids are hydrophobic insoluble molecules and, therefore, travel through the aqueous blood in lipoprotein vesicles composed of a phospholipid monolayer and proteins called apoproteins.[17] Apoproteins wrap around the outside of the phospholipid monolayer using α-helices with hydrophobic residues oriented inside the hydrophobic lipid monolayer and hydrophilic residues interacting with the polar lipid head groups. Apoproteins bind cell surface receptors and allow direct tissue-specific transport of the lipids contained within the lipoprotein vesicles. Two types of lipoproteins are known to transport triacylglycerols. Very low-density lipoproteins (LDL) transport newly synthesized triacylglycerol from the liver to adipose tissue, and chylomicrons

FIGURE 1.5 Lipoproteins transport lipids within vesicles composed of a phospholipid monolayer and apoproteins.

transport triacylglycerol to the liver, skeletal muscle, and adipose tissue. Cholesterol is transported inside two other types of lipoproteins. LDL transport cholesterol from the liver to different cells of the body, and high-density lipoproteins (HDL) recycle this cholesterol back to the liver (Figure 1.5).

1.4 Organelle Cell Membranes

Like the cell itself, cytoplasmic organelles are surrounded by complex mixtures of lipids and proteins. Importantly, these organelles compartmentalize a great number of reactions that affect bioenergetics and lipid homeostasis.

1.4.1 Mitochondria

Mitochondria have an outer membrane and an infolded inner membrane with roughly five times the surface area of the outer membrane.[19] The inner membrane space exists between the outer and inner membranes and the matrix exists within the inner membrane. Cristae are the small regions formed within the folds of the inner membrane. The outer membrane contains porin channels composed of the β-sheet secondary structure of integral membrane proteins. These porins are relatively large and allow the passage of molecules smaller than ~5000 Da. In contrast, the inner membrane is highly impermeable, possibly because of the presence of cardiolipin (bisphosphatidyl glycerol). Cardiolipin is a lipid with four fatty acid tails and is only found within the membranes of mitochondria and some prokaryotes.[18] Cardiolipin comprises approximately 20% of the inner membrane of mitochondria and, through its four fatty acid tails, creates a highly impermeable barrier that facilitates proton-gradient formation. Mitochondria also have a small circular genome that encodes a little less than 40 genes.[19] These genes code for ribosomal RNA (rRNA), transfer RNA (tRNA), and protein components of the electron transport system. Within the matrix, the electron transport proteins couple the oxidation of carbohydrates and fatty acids to proton-gradient formation and ATP generation.

1.4.2 Peroxisomes

These organelles are delimited by a single membrane lipid bilayer that compartmentalizes oxidative metabolic reactions.[19] During β-oxidation of fatty acids, enzymes of the peroxisome progressively shorten the hydrocarbon tails of fatty acids by two carbon units, each of which is used to make one molecule of acetyl CoA. Therefore, when a fatty acid with 16 carbons is oxidized in this manner, eight molecules of acetyl CoA are produced. These acetyl-CoA molecules can then be transported to the mitochondria and used to fuel ATP production. Peroxisomes also contain the enzyme catalase, which converts hydrogen peroxide, a by-product of these β-oxidation reactions, into water and molecular oxygen. Catalase also detoxifies alcohol, phenols, formic acid, and formaldehyde.

1.4.3 Lysosomes

These membrane-bound organelles contain different types of acid hydrolases, including lipases, phospholipases, phosphatases, and sulfatases, that use hydrolysis to sever the bonds of numerous cellular materials.[19] Catalytic activity of these enzymes requires an acidic environment of about 5.0, which is produced by membrane-bound H+ ATPase that pumps protons from the cytosol into the lumen of the lysosome. These hydrolases serve to digest the macromolecules that are delivered to lysosomes during endocytic processes (see Section 1.5).

1.4.4 ER and Golgi

Translation of all proteins begins on free ribosomes in the cytoplasm.[19] Those destined for secretion, the plasma membrane, lysosome, ER, or Golgi must first enter the ER. These proteins are either deposited entirely within the lumen of the ER or inserted as transmembrane proteins, depending on the function that each serves in its final destination. Within the ER environment, proteins can be glycosylated and modified with glycolipid anchors and/or disulfide bonds. Chaperone-assisted protein folding and assembly into multisubunit complexes also occur within the ER. Following those modifications, these proteins bud from the ER within vesicles that then fuse with the membrane-enclosed sacs of the Golgi. Further rounds of glycosylation occur within the Golgi stacks before the protein is packaged into vesicles that fuse with the plasma membrane, lysosome, or ER. These vesicles travel along microtubules to their final destination, which is determined by receptor-mediated interactions at vesicle/membrane interfaces. For example, vesicles destined for the plasma membrane have receptors that only interact with those on the cytoplasmic surface of the plasma membrane.

Lipid synthesis also occurs inside the ER and the Golgi.[19] Phospholipids, cholesterol, and ceramide are synthesized in the ER, while enzymes within the Golgi utilize ceramide to produce sphingolipids and glycolipids. Transport of these lipids will depend on the current demands of the cell or organism.

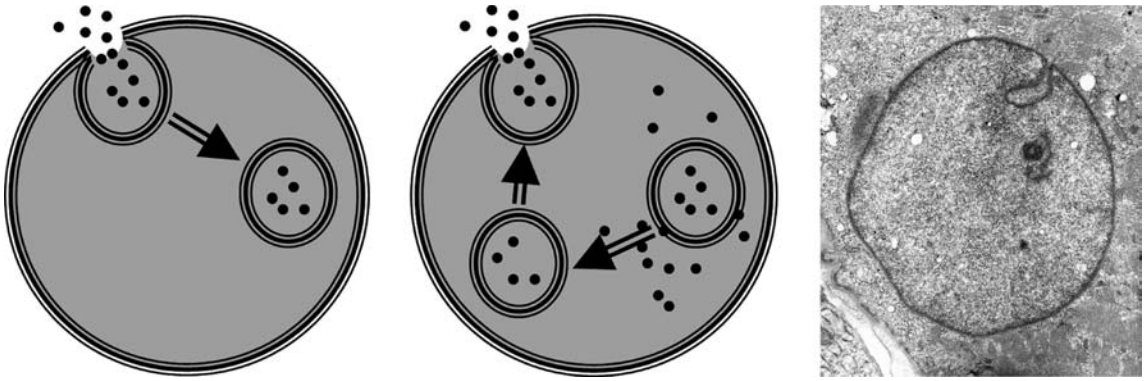

FIGURE 1.6 Endocytosis (left), exocytosis (middle), and phagocytosis. (TEM courtesy of Winston Wiggins, Daisy Ridings, and Alicia Roh, Carolinas HealthCare System, 1000 Blythe Blvd. Charlotte NC.)

1.5 Vesicle Transport

A highly interconnected series of vesicle transport routes mediates the exchange of materials among organelles, as well as between the cell and its environment. Phagocytosis, pinocytosis, clathrin-mediated endocytosis, and caveolae-dependent uptake are mechanisms of endocytosis used during vesicular internalization.[20] Conversely, the process by which materials are delivered from within the cell to the plasma membrane occurs during exocytosis.[21] Together, endocytosis and exocytosis influence membrane surface area homeostasis and the recycling of cellular materials that includes transmembrane receptors and lipids (Figure 1.6).

1.5.1 Phagocytosis

Phagocytosis occurs when large particles, like bacteria or dead cells, are internalized after binding the cellular receptors of phagocytes (e.g., macrophages and neutrophils).[20] Binding results in actin-dependent clustering of the receptors and pseudopodia extension of actin filaments, so that the object becomes surrounded within a large phagosome derived of plasma membrane. During fusion with the lysosome, ligand/receptor interactions are broken within the acidic environment. The receptors can then be placed in new vesicles that return and fuse with the plasma membrane in an effort to recycle these surface receptors. Interestingly, some pathogenic bacteria are able to escape before the phagosome fuses with the lysosome, while others can survive the acidic environment of the lysosome.

1.5.2 Pinocytosis

Pinocytosis, or cell drinking, allows cells to internalize extracellular fluid that may contain nutrients in bulk.[20] It is an actin-dependent process that does not follow a receptor-mediated mechanism. However, pinocytosis may be initiated by upstream pathways that respond to growth factor or hormone signaling. The internalized extracellular fluid is typically transported to the lysosome, where it is metabolized.

1.5.3 Clathrin-Mediated Endocytosis

Clathrin-mediated endocytosis permits the uptake of essential nutrients and the internalization of activated receptors from the cell surface. With regard to receptors, such internalization may down-regulate or modify their activity at the plasma membrane, or allow them to participate in signal transduction cascades within the cell.[22] Clathrin forms a hexameric complex of three 190-kDa heavy chains and two 30-kDa light chains that assemble on adapter molecules located at the cytoplasmic surface of the plasma membrane.[23] Assembly results in the production of a cage (50–100 nm in diameter) that engulfs and coats the membrane invagination. Dynamin is a large 100-kDa guanosine triphosphate (GTPase) that assembles around the neck of the clathrin-coated pit and, upon GTP hydrolysis, constricts the membrane to release the clathrin-coated vesicle. This clathrin coat is later removed from the vesicle and recycled to other adapter molecules as the vesicle is transported to the lysosome.

1.5.4 Caveolae-Dependent Endocytosis

Caveolae-dependent endocytosis[24,25] also facilitates the uptake of essential nutrients and receptors. Caveolins are proteins that localize to lipid rafts, which are small regions of the outer plasma membrane particularly enriched in cholesterol and sphingolipids. Many caveolins weave through the lipid bilayer of these rafts, forming loops as both N- and C-termini remain on the cytoplasmic surface of the membrane. This caveolin scaffold may influence the size and shape of the membrane region to be internalized, a region that has a diameter of 50–80 nm. Like clathrin-dependent endocytosis, caveolae are internalized by a mechanism that depends on dynamin. These caveolin-decorated vesicles are delivered to lysosomes or possibly a different place within the cell or plasma membrane.

1.5.5 Exocytosis

Exocytosis describes the vesicular transport of cellular materials to the plasma membrane.[19] These vesicles may originate from

the lysosome, ER, Golgi, or another region of the plasma membrane. If transported in the lumen of the vesicles, this material is secreted from the cell and used to build the extracellular matrix, communicate with other cells, or remove waste. If transported within vesicle membranes, this material will become incorporated into the plasma membrane.

1.5.6 Cytoskeleton

The cytoskeleton establishes and maintains many of the structural characteristics and mechanical activities of cells.[19] In terms of structure, proteins of the cytoskeleton form cables (Figure 1.7) that interact directly and indirectly with cellular membranes to establish and maintain a diverse array of cellular architectures. Meanwhile, mechanical activities of the cytoskeleton usually depend on their interactions with a variety of different motor proteins.

1.5.6.1 Assembly of the Cytoskeleton

The cytoskeleton is composed of filamentous actin (F-actin), microtubules, and intermediate filaments (IFs), all of which are composed of repeating protein subunits. ATP-bound globular actin monomers (G-actin) stack end-on-end to produce F-actin cables, while GTP-bound tubulin dimers (α and β tubulin) stack end-on-end to produce microtubule cables. The assembly of each cable is regulated by a large number of proteins; some of these serve as nucleation platforms and others regulate the state of the nucleotide cofactor. The state of the nucleotide cofactor is important because nucleotide triphosphate-bound states are required for assembly while diphosphate-bound states tend to promote disassembly of these cables. IFs are composed of repeating protein subunits with coiled-coil structure. Unlike F-actin and microtubules, IF assembly does not appear to be regulated by a nucleotide cofactor.

1.5.6.2 Cytoskeletal Functions

All three filaments support the morphological architecture of cells, but only actin and microtubule filaments are known to directly participate in mechanical processes.[19] This seems to be due to their ability to interact with motor proteins. Motor proteins consist, with a few exceptions, of a head domain, a heavy chain, and a regulatory light chain. The head domain is an ATPase motor that steps along the length of the filament during ATP hydrolysis by a not yet fully resolved molecular mechanism. The heavy chain associates with cargo while both the heavy and light chains are subject to post-translational modifications that exert regulatory control over movement and cargo affinity. Some motors have two head domains, in which case physical interactions among heavy and/or light chains tether these domains together. These motors transport numerous types of cargo along cytoskeletal cables, including mitochondria and both endocytotic and exocytotic vesicles.

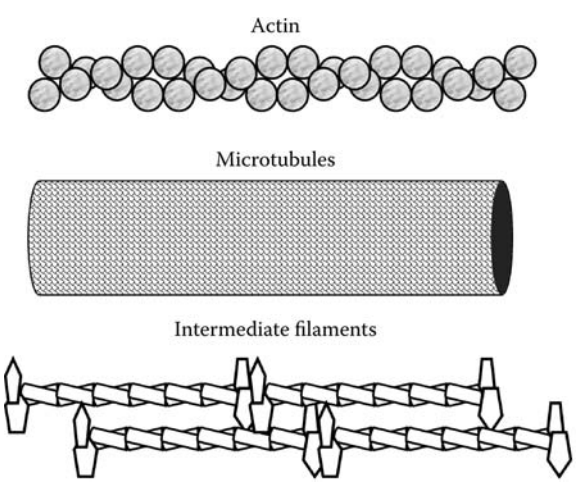

FIGURE 1.7 The cellular cytoskeleton.

1.6 Motor Proteins

1.6.1 Kinesins, Dyneins, and Myosins

Kinesins and dyneins are microtubule-dependent motor proteins that step toward opposite ends of the microtubule cables. Both these mechanochemical enzymes have a pair of motor domains that take overlapping, hand-over-hand steps along the microtubule surface. *In vitro* measurements suggest that these head domains take 8 nm steps and generate ~6 pN of peak force during one ATP hydrolysis cycle.[26,27] ATP-dependent velocities of single kinesin molecules follow the Michaelis–Menten relationship shown in Equation 1.6:

$$v(c) = \frac{v_{\max} c}{K_m} + c, \quad (1.6)$$

where K_m is the mechanochemical Michaelis–Menten constant, c is the ATP concentration, and $v_{\max}$ is the velocity at saturating ATP concentration.[28]

Myosins are one- and two-headed actin-dependent motors with step sizes between 5 nm and >40 nm.[29] Two-headed isoforms like Myosin II participate in contractile assemblies that influence sarcomere length in muscle cells and actomyosin ring constriction during cytokinesis of dividing cells.[19] Within these contractile assemblies, Myosin II tails physically associate with each other to form myosin filaments. The head domains of these filaments associate with actin filaments of different polarity. Because the orientation of these myosins reverses along the myosin filaments, ATP hydrolysis by the motor domains causes the actin filaments to slide toward each other. The force generated by each myosin molecule adheres to the following relationship, where force (F) relates to the bending stiffness (Ei) and length (L) of the tail domains that is expressed in Equation 1.4[30]:

$$F = \frac{3Ei}{L^2}. \quad (1.7)$$

In contrast to Myosin II, one-headed myosins do not have tails that form coiled-coils and therefore do not participate in contractile mechanisms. Instead, the tails of these myosins bind vesicles and organelles in order to transport them along actin filaments.

References

1. Hamill OP and Martinac B. Molecular basis of mechanotransduction in living cells. *Physiol Rev* 2001, 81: 685–740.
2. Henon S, Lenormand G, Richert A, and Gallet F. A new determination of the shear modulus of the human erythrocyte membrane using optical tweezers. *Biophys J* 1999, 76: 1145–1151.
3. Lenormand G, Henon S, Richert A, Simeon J, and Gallet F. Direct measurement of the area expansion and shear moduli of the human red blood cell membrane skeleton. *Biophys J* 2001, 81: 43–56.
4. Lenormand G, Henon S, Richert A, Simeon J, and Gallet F. Elasticity of the human red blood cell skeleton. *Biorheology* 2003, 40: 247–251.
5. Martin S and Parton RG. Lipid droplets: A unified view of a dynamic organelle. *Nat Rev Mol Cell Biol* 2006, 7: 373–378.
6. van Meer G, Voelker DR, and Feigenson GW. Membrane lipids: Where they are and how they behave. *Nat Rev Mol Cell Biol* 2008, 9: 112–124.
7. Barnett-Norris J, Lynch D, and Reggio PH. Lipids, lipid rafts and caveolae: Their importance for GPCR signaling and their centrality to the endocannabinoid system. *Life Sci* 2005, 77: 1625–1639.
8. Simons K and Vaz WL. Model systems, lipid rafts, and cell membranes. *Annu Rev Biophys Biomol Struct* 2004, 33: 269–295.
9. Moffett S, Brown DA, and Linder ME. Lipid-dependent targeting of G proteins into rafts. *J Biol Chem* 2000, 275: 2191–2198.
10. Sens P and Turner MS. The forces that shape caveolae. In J. Fielding (Ed.), *Lipid Rafts and Caveolae*. Wiley-VCH Verlag GmbH & Co, 2006.
11. Roduit C, van der Goot FG, De Los Rios P, Yersin A, Steiner P, Dietler G, Catsicas S, Lafont F, and Kasas S. Elastic membrane heterogeneity of living cells revealed by stiff nanoscale membrane domains. *Biophys J* 2008, 94: 1521–1532.
12. Yersin A, Hirling H, Kasas S, Roduit C, Kulangara K, Dietler G, Lafont F, Catsicas S, and Steiner P. Elastic properties of the cell surface and trafficking of single AMPA receptors in living hippocampal neurons. *Biophys J* 2007, 92: 4482–4489.
13. Luu DT, Marty-Mazars D, Trick M, Dumas C, and Heizmann P. Pollen-stigma adhesion in *Brassica* spp involves SLG and SLR1 glycoproteins. *Plant Cell* 1999, 11: 251–262.
14. Vliegenthart JF and Casset F. Novel forms of protein glycosylation. *Curr Opin Struct Biol* 1998, 8: 565–571.
15. Wei X and Li L. Comparative glycoproteomics: Approaches and applications. *Brief Funct Genomic Proteomic* 2009, 8(2): 104–113.
16. Wells L and Hart GW. O-GlcNAc turns twenty: Functional implications for post-translational modification of nuclear and cytosolic proteins with a sugar. *FEBS Lett* 2003, 546: 154–158.
17. Zubay GI. *Biochemistry*, 4th edition. Dubuque, IA: Win C. Brown, 1998.
18. Schlame M. Cardiolipin synthesis for the assembly of bacterial and mitochondrial membranes. *J Lipid Res* 2008, 49: 1607–1620.
19. Cooper GM and Hausman RE. *The Cell: A Molecular Approach*, 4th edition. Sunderland, MA: Sinauer Associates, Inc, 2007.
20. Doherty GJ and McMahon HT. Mechanisms of Endocytosis. *Annu Rev Biochem* 2009, 78: 857–902.
21. Lin RC and Scheller RH. Mechanisms of synaptic vesicle exocytosis. *Annu Rev Cell Dev Biol* 2000, 16: 19–49.
22. Felberbaum-Corti M, Van Der Goot FG, and Gruenberg J. Sliding doors: Clathrin-coated pits or caveolae? *Nat Cell Biol* 2003, 5: 382–384.
23. Ungewickell EJ and Hinrichsen L. Endocytosis: Clathrin-mediated membrane budding. *Curr Opin Cell Biol* 2007, 19: 417–425.
24. Nichols BJ and Lippincott-Schwartz J. Endocytosis without clathrin coats. *Trends Cell Biol* 2001, 11: 406–412.
25. Parton RG. Caveolae and caveolins. *Curr Opin Cell Biol* 1996, 8: 542–548.
26. Svoboda K, Mitra PP, and Block SM. Fluctuation analysis of motor protein movement and single enzyme kinetics. *Proc Natl Acad Sci USA* 1994, 91: 11782–11786.
27. Svoboda K, Schmidt CF, Schnapp BJ, and Block SM. Direct observation of kinesin stepping by optical trapping interferometry. *Nature* 1993, 365: 721–727.
28. Howard J, Hudspeth AJ, and Vale RD. Movement of microtubules by single kinesin molecules. *Nature* 1989, 342: 154–158.
29. Yanagida T and Iwane AH. A large step for myosin. *Proc Natl Acad Sci USA* 2000, 97: 9357–9359.
30. Tyska MJ and Warshaw DM. The myosin power stroke. *Cell Motil Cytoskeleton* 2002, 51: 1–15.

2

Protein Signaling

Sonja Braun-Sand

2.1 Modeling Electrostatics in Proteins

Maxwell's equations describe the properties of electric and magnetic fields, and have been analytically solved for some simple cases. However, calculation of electrostatics in proteins is not a trivial problem, and several models have been used to try to describe these interactions. The question is of extreme interest, however, because electrostatic energies are one of the best correlators between structure and function in biochemical systems.[1–4] There are two main problems in formulating a model to describe protein electrostatics.[5] First, the electrostatic interactions within proteins are occurring at microscopically small distances, which make the dielectric constant ambiguous. In addition, the protein environments are irregularly shaped, such that the analytical models are impractical to use.

Microscopic studies of electrostatics in proteins have emerged with the increase in availability of x-ray crystal structures of proteins and the realization that electrostatic energies provide one of the best ways to correlate structure with function. Many mathematical descriptions of electrostatics in proteins have been proposed, and all are based on Coulomb's law, which gives the reversible work of bringing two charges close together as represented by Equation 2.1:

$$\Delta W = 332\frac{Q_i Q_j}{r_{ij}}, \tag{2.1}$$

where the distance, r, is given in Å, the charge Q is in atomic units, and the free energy, W, is in kcal/mol. Manipulations of this equation[5] lead to the Poisson equation, Equation 2.2:

$$\nabla^2 U(r) = -4\pi\rho(r), \tag{2.2}$$

where the electric field, $\mathbf{E}$, is expressed as a gradient of the scalar potential, U, and ρ is the charge density. By assuming that a dielectric constant can be used to express effects not treated explicitly, the following equation is reached (Equation 2.3):

$$\nabla\varepsilon(\mathbf{r})\nabla^2 U(\mathbf{r}) = -4\pi\rho(\mathbf{r}). \tag{2.3}$$

If it is assumed that the ion distribution follows the Boltzmann distribution, the linearized Poisson–Boltzmann equation is reached, given by Equation 2.4:

$$\nabla\varepsilon(\mathbf{r})\nabla^2 U(\mathbf{r}) = -4\pi\rho(\mathbf{r}) + \kappa^2 U, \tag{2.4}$$

where κ is the Debye–Huckel screening parameter.

Interesting questions arise when these equations are applied to biological systems. For example, can a dielectric constant be applied to heterogeneous systems, such as an enzyme active site? In addition, are continuum assumptions valid on a molecular level? An early work, the Tanford Kirkwood[6] model, described a protein as a sphere with a uniform dielectric constant. This model was proposed before protein structures were known, and it was thought that ionizable residues were located solely on the protein exterior. Later studies conducted after many protein structures had been elucidated found that the simplification of a protein as a uniform dielectric constant missed some important aspects of the physics of charged residues in a protein interior.[7] Discussed below are alternative approaches to describing the electrostatics of protein interiors.

2.1.1 Theory and Models

Electrostatic models span a wide range of possibilities from continuum dielectric approaches[1,8,9] to all-atom models that explicitly represent the biological molecule and solvent.[10,11] Each model has its own advantages and disadvantages.[5,12–15] There are three primary ways of describing solvent in a system, shown in Figure 2.1.[16] Simulation time decreases from the microscopic all-atom model to the macroscopic model.

2.1.1.1 Protein Dipoles Langevin Dipoles Model

A microscopic dipolar model that is often used in simulations of biological molecules is the protein dipoles Langevin dipoles (PDLD) model.[17,18] This model does not assume a dielectric constant for the solvent molecules; rather, the time-averaged

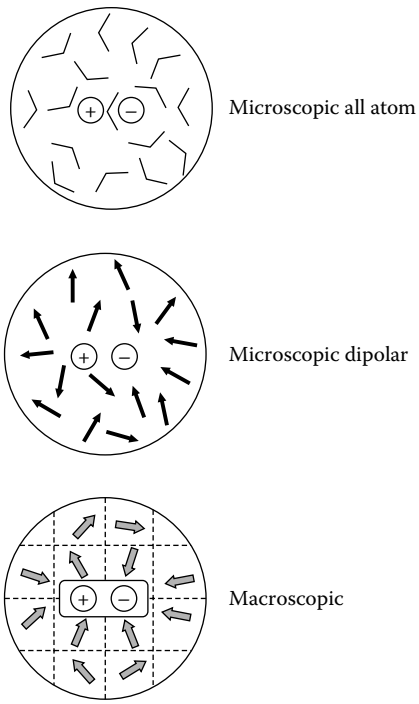

FIGURE 2.1 Three approaches to solvent representation. All atoms are represented in the microscopic approach. A point dipole is used to represent a solvent molecule in the dipolar approach, and several solvent molecules within a certain volume are represented as a polarization vector in the macroscopic approach.

polarization of each solvent molecule is represented as a Langevin dipole.[17,18] The dipoles are placed in a spherical grid, rather than attempting to reproduce the exact locations of the solvent molecules. The net polarization of a thermally fluctuating dipole in response to an electric field is described by the following equations.[16]

$$(\mu_i^{\mathrm{L}})^{n+1} = e_i^n \mu_0 \left(\coth(x)_i^n - \frac{1}{x_i^n} \right), \tag{2.5}$$

where x_i^n is described by

$$x_i^n = \frac{C' \mu_0}{k_{\mathrm{B}} T} \left| \xi_i^n \right|, \tag{2.6}$$

and where ξ_i^n is the local field, μ_0 is 1.8 debye, e_i^n is a unit vector in the direction of the local field, C' is a parameter, and the superscript $(n+1)$ indicates that the equation is solved iteratively.

2.1.1.2 Protein Dipoles Langevin Dipoles/ Semimacroscopic-Linear Response Approximation Model

The microscopic PDLD model discussed above does not use any dielectric constants. A potential problem with these types of methods is poor convergence of results. One solution to this problem is to scale the dipole contributions of the PDLD model with an assumed protein dielectric constant, ε_{p}, leading to a semimacroscopic PDLD (PDLD/S) model.[16,19] (For discussions of dielectric constants in proteins, see Refs. [20–22]). To aid in the description of ε_{p}, the linear response approximation (LRA) is used. In order to apply the LRA approximation, a molecular dynamics (MD) simulation is done to generate a number of protein configurations for the charged and uncharged states of the solute of interest. The LRA approximation uses a thermodynamic cycle to evaluate the PDLD/S energy by averaging over the configurations (with solute charged and uncharged) generated by the MD simulations.[18] This approach is summarized in Figure 2.2, taken from the *Molaris Manual and User Guide*.[16] It is difficult to go from A to B directly; hence a thermodynamic cycle from A → D → C → B is used.

The thermodynamic cycle in Figure 2.2 leads to the following equation, which gives the difference in solvation energy when moving a charge from water to a protein active site shown in Equation 2.7:

$$\Delta\Delta G_{\mathrm{sol}}^{\mathrm{w}\to\mathrm{p}} = \tfrac{1}{2}[\langle \Delta U^{\mathrm{w}\to\mathrm{p}}(Q=0 \to Q=Q_0)\rangle]_{Q_0} + \langle \Delta U^{\mathrm{w}\to\mathrm{p}}(Q=Q_0)\rangle_{Q=0}, \tag{2.7}$$

where

$$\Delta U^{\mathrm{w}\to\mathrm{p}} = \left[\Delta\Delta G_{\mathrm{p}}^{\mathrm{w}}(Q=0 \to Q=Q_0) - \Delta G_Q^{\mathrm{w}} \right] \left(\frac{1}{\varepsilon_{\mathrm{p}}} - \frac{1}{\varepsilon_{\mathrm{w}}} \right) + \Delta U_{Q\mu}^{\mathrm{p}}(Q=Q_0) \frac{1}{\varepsilon_{\mathrm{p}}}, \tag{2.8}$$

where the subscripts and superscripts p and w refer to protein and water, respectively, ΔG_Q^{w} is the solvation energy of the charge, Q, in water, $\Delta\Delta G_{\mathrm{p}}^{\mathrm{w}}$ is the change in solvation energy of the protein and bound charge upon changing Q from Q_0 to 0, and $\Delta U_{Q\mu}^{\mathrm{p}}$ is the electrostatic interaction between polar protein groups and the charge.

2.1.1.3 Interactions of Ions with Membrane Proteins

An application of the protein dipoles Langevin dipoles/semimacroscopic-linear response approximation (PDLD/S-LRA) model (in conjunction with a microscopic determination of the free energy profile for ion transport) is demonstrated in a study of the ion selectivity of the KcsA potassium channel.[23] Remarkably, this ion channel has the ability to discriminate between K^+ and Na^+ ions, allowing K^+ ions to pass through ~1000 times more readily.[24,25] Crystallographic structures are available for this transmembrane protein from *Streptomyces lividans*,[26,27] enabling many computational estimates, using a variety of methods, of the selectivity barrier.[28–33] With the present computing power, the system is too large to allow direct MD simulations of ion transport in a reasonable time. Use of the PDLD/S-LRA model

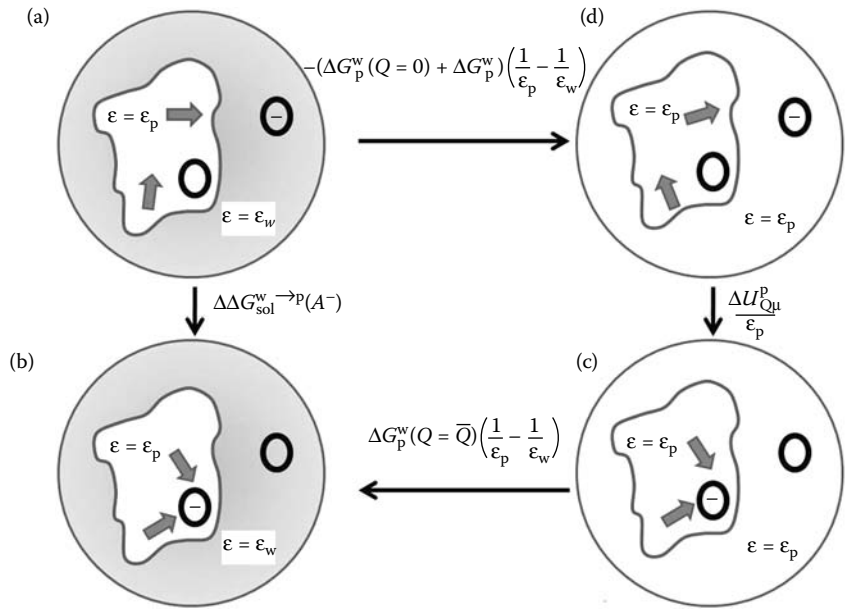

FIGURE 2.2 The PDLD/S-LRA thermodynamic cycle for evaluation of $\Delta\Delta G_{sol}^{w\to p}(A^-)$.

enables simulation of the K^+ and Na^+ ion currents in a reasonable time in this large system. The simulation system was essentially cylindrical, with a diameter of ~40 Å, which included the channel protein and a small portion of the membrane, and a length of ~89 Å, which included the length of the protein, 30 Å intracellular space, and 25 Å extracellular space. The study was able to examine the effects of several variables on ion current, including the effective dielectric constant used for the protein (which varied from 15 to 30), and the friction for moving the ion through the channel.

What were the factors found by this study to be most important in determining ion selectivity through the channel? First, the study found differences in channel radius at the initial ion loading sites based on the presence of K^+ or Na^+. This led to different geometries, and thus different channel reorganization energies for the ions. This reorganization energy can be captured with the PDLD/S-LRA model because it effectively evaluates the steric interactions between the ion and the channel. Second, it was found that the calculated free energy profiles were very sensitive to the protein dielectric constant, ε_p, used. In this case a large effective dielectric constant for the protein is necessary to properly represent the charge–charge interactions, if the LRA approximation is not used. A typical protein dielectric constant, ε_p, used in many studies without the LRA approximation is less than 6, but this low ε_p may not correctly evaluate charge–charge interactions ($\Delta U_{Q\mu}^p$ in Equation 2.8). The strong dependence of the energy profile on the protein dielectric used may be due in part to the narrow protein channel through which the ions pass. Because the KcsA channel is so narrow, the ion is probably not solvated on all sides by water molecules, as it would be in wider channels, such as porins. This may make interactions with the protein, and thus the value of ε_p, much more important in the calculations.

2.1.2 Bacteriorhodopsin, a Transmembrane Protein

Transmembrane proteins span the width of a lipid bilayer, and have many uses within an organism. For example, transmembrane proteins may be used as ion or water channels, transporters, receptors in signal transduction pathways, proton pumps in the electron transport chain (ETC), adenosine triphosphate (ATP) synthases, and many others. The largest class of cell surface receptors is the seven-transmembrane helix (7TM) family. It is estimated that ~50% of therapeutic drugs on the market today target members of this family. A well-known example of this family is bacteriorhodopsin (bR). bR is present in the membranes of some halobacteria. It harvests light energy and then converts it to electrostatic energy in the form of proton transport (PTR) out of the cell. This creates a large pH gradient across the cell membrane, which is then used to create ATP when the cell allows a proton to move back into the cell, through another transmembrane protein, ATP synthase.

2.1.2.1 Empirical Valence Bond Model

Often scientists want to study biochemical bond breaking and forming processes, such as the breaking of a covalent bond to H, and the forming of a new covalent bond to H. Modeling these types of chemical reactions requires the use of a quantum mechanical (QM) treatment to describe the reacting fragments, coupled with a classical, molecular mechanics (MM) simulation of the surrounding biological molecule (where no reactions are taking place), resulting in a quantum mechanics/molecular mechanics (QM/MM) method. Frequently, a molecular orbital-based QM treatment, which is, for example, very effective for calculating spectroscopic properties of molecules, is prohibitively expensive when studying biochemical systems. An alternative

to using molecular orbital-based QM methods is the empirical valence bond (EVB) model,[34] which is effective at calculating bond rearrangements.

The EVB method first calculates the ground state potential energy surface of reacting fragments by mixing the valence bond (VB) resonance structures of the reactants and products. The reaction is forced to occur by gradually moving the wave function from 100% reactant, 0% product to 0% reactant, 100% product. The portion of the molecule described by MM adjusts itself to the reacting fragments in order to minimize the overall energy of the reaction. Importantly, this method is not as expensive as methods that use a molecular orbital QM approach, and allows sufficient configurational averaging to give the overall free energy change for the system.[34,35]

An important point to be made about the EVB model is that the reaction simulation must be carried out both in water and in the protein. The simulations begin in water, where the energetics of the reaction are known. For proton transfer (PT) reactions, the change in free energy of the PT in water can be obtained if one knows the pK_a values of the donor (DH^+) and the protonated acceptor (AH) in water. This is given in kcal/mol by Equation 2.9:

$$\Delta G^{w}_{PT}(DH^+ + A^- \rightarrow D + AH)_\infty = 1.38(\Delta pK^{w}_a), \qquad (2.9)$$

where ∞ indicates that the donor and acceptor are at large separation. All of the adjustable parameters used in the EVB model of the reaction are adjusted so that the water simulation of the PT between donor and acceptor at large separation in water reproduces the experimentally known difference in pK_a values. The parameters are then fixed, and not allowed to vary when moving to simulations of the reaction in the biochemical system. An example where the EVB method was used in bR is given below.

2.1.2.2 Conversion of Light Energy to Electrostatic Energy

The mechanism of light-induced PTR across a membrane and against a proton gradient is of significant interest in bioenergetics.[36–47] bR is a well-characterized model system for this process, with many structures available of the ground state and several intermediates, and many kinetic studies having been performed with it.[36,48–50] This structural information was recently used to propose a detailed molecular picture of how bR converts light energy to electrostatic energy. In the active site, the chromophore is covalently attached to an arginine side chain through a protonated Schiff base (SB), and it forms an ion pair with the negatively charged side chain of Asp85.[51–53] It is known that bR absorbs light, and then a sequence of relaxation and PTR processes occurs, ultimately resulting in a proton being transported outside of the cell. However, the driving force for the initial PT from the SB to the Asp85 was unclear. A previous study[54] and a more recent study[47] suggest that the PT is driven by a light-induced charge separation of the ion pair. Apparently the absorption of a photon by the chromophore leads to isomerization around a carbon–carbon double bond and a high energy, sterically strained ground state. Relaxation of this steric energy leads to the increase in ion pair distance observed in structural and computational studies, ultimately leading to the PT.

2.1.2.3 Modeling the Conversion of Light Energy to Electrostatic Energy

The computational methods used in the more recent study[47] to convert structural information to free energy barriers for the PT process are described here. First, calculation of the PT potential energy surface in the ground state and several of the photocycle intermediates was performed to obtain the free energy landscape for the system. (For an in-depth description of the photocycle, see Refs. [36,55].) This study used a type of QM/MM method that combines the quantum consistent force field/pi electrons (QCFF/PI) method[56] and the EVB[35] approach. An *ab initio* QM/MM method was not used because the calculations to do the proper configurational averaging needed to provide reliable free energy surfaces are prohibitively expensive. The energetics of the PT are modeled by considering two VB resonance structures of the form

$$\begin{aligned} \Psi_1 &= R{\cdots}C(H){=}N^+(R')H^-A \\ \Psi_2 &= R{\cdots}C(H){=}N^+(R')H{-}A \end{aligned} \qquad (2.10)$$

where the wavefunction Ψ_1 represents the protonated SB (SBH^+) and deprotonated acceptor, A^- (Asp85), and Ψ_2 represents the deprotonated SB and protonated acceptor (Asp-H). Because the chromophore contains many pi electrons, the SB is represented by the QCFF/PI potential surface, and the acceptor is represented by an empirical potential function (as in the normal EVB). Water and protein surrounding the reacting system are coupled to the QCFF/PI Hamiltonian through a standard QM/MM treatment. This analysis allows the system to be represented by two diabatic or pure states, with the conditions outlined by Equation 2.11:

$$\begin{aligned} \bar{\varepsilon}^{(1)} &= \varepsilon_{QCFF/PI}(SBH^+) + \varepsilon'_{Asp85} + \varepsilon^{(1)}_{SS'} + \varepsilon^{(1)}_{Ss} + \varepsilon_{ss} + \alpha^{(1)}, \\ \bar{\varepsilon}^{(2)} &= \varepsilon_{QCFF/PI}(SB) + \varepsilon'_{AspH85} + \varepsilon^{(2)}_{SS'} + \varepsilon^{(2)}_{Ss} + \varepsilon_{ss} + \alpha^{(2)}, \end{aligned} \qquad (2.11)$$

where the $\varepsilon_{QCFF/PI}$ of the indicated form of the chromophore includes the potential from the solvent/protein system, ε' is an EVB description of Asp85 or AspH85, and $\varepsilon_{SS'}$ is the interaction between the classical (EVB) and π-electron systems, which is being treated as in the regular EVB treatment by considering the classical electrostatic and steric interactions between the two fragments. Finally, $\varepsilon^{(i)}_{Ss}$ represents the interaction between the solute (S) and the solvent (s) in the given state, while $\alpha^{(i)}$ is the "gas phase shift." The gas phase shift is a parameter that is adjusted by requiring that the PT at large separation in water between SBH^+ (pK_a = 7.0) and Asp (Asp-H pK_a = 4.0) reproduce

the experimental pK_a difference of 3.0 pH units (corresponding to 4.1 kcal/mol). The pure diabatic states shown above do not reflect the actual ground state potential energy surface of the system, which is represented by mixing the two diabatic states according to Equation 2.12:

$$E_g = \frac{1}{2}\left[(\varepsilon^{(1)} + \varepsilon^{(2)}) - \left((\varepsilon^{(1)} + \varepsilon^{(2)})^2 + 4H_{12}^2\right)^{1/2}\right], \qquad (2.12)$$

where H_{12} is the off-diagonal coupling element between Ψ_1 and Ψ_2.

It should be emphasized that all of the required parameters, such as the gas phase shift, are adjusted during the simulation of PT from SBH^+ to Asp in water, requiring that the values used reproduce experimental results. The parameters are then fixed, and are not adjusted in protein simulations.

In moving to the protein simulations, it was found that the driving force for the initial PT from SBH^+ to Asp is primarily based on electrostatic effects. The absorption of a photon by the chromophore leads to a sterically strained structure. Relaxation of this strain leads to destabilization of the ion pair by increasing the ion pair (SBH^+Asp) distance, ultimately driving the PT process. The difference in energy between the ion pair and the neutral state seemed to determine the majority of the barrier to the PT process.

2.1.3 Coupling between Electron and Proton Transport in Oxidative Phosphorylation

Peter Mitchell was awarded the 1978 Nobel Prize for Chemistry for his revolutionary chemiosmotic hypothesis (see Refs. [39,57]). This theory stated that ATP synthesis by the oxidative phosphorylation pathway is coupled to PTR from the cytoplasmic side to the matrix side of the inner mitochondrial membrane. It is now known that transfer of high-energy electrons from the citric acid cycle (from NADH and $FADH_2$) to complexes of the ETC (which are embedded in the inner mitochondrial matrix) results in reduction of an electron acceptor, O_2, to H_2O. In eukaryotes, there are four transmembrane complexes involved in the ETC, three of which are also proton pumps. Complex I (NADH-Q oxidoreductase), Complex III (Q-cytochrome *c* oxidoreductase), and Complex IV (cytochrome *c* oxidase) all pump protons, with a stoichiometry of 2, 2, and 1 H^+ per high-energy electron.[58] Only Complex II (succinate-Q reductase) does not. This electron transfer (ET) also leads to the creation of a proton gradient across the membrane, creating a proton motive force (*PMF*), which consists of two parts, a chemical gradient and a charge gradient as expressed by Equation 2.13[58]:

$$\mathrm{PMF}(\Delta p) = \text{chemical gradient}(\Delta \mathrm{pH}) + \text{charge gradient}(\Delta\Psi). \qquad (2.13)$$

The PMF can be used to drive the synthesis of ATP when protons are allowed to move back into the matrix through ATP synthase (sometimes called Complex V). The typical pH difference across the membrane is around 1.4 pH units (outside is more acidic), and the membrane potential is about 0.14 V (outside is positive), leading to a free energy of 5.2 kcal/mol of electrons.[58]

2.1.3.1 Electron Transport Chain Complexes as Proton Pumps

Similar to the KcsA ion channel and bR proteins discussed previously, complexes of the ETC are embedded in a membrane. While there have been several experimental and theoretical studies of ET[59–63] and PT[64–67] individually in proteins, there have been fewer studies of coupled ET/PT reactions.[68–71]

An extensive theoretical analysis of coupled ET and PT in Complex IV of the ETC, cytochrome *c* oxidase, has been published.[72] Many of the ETC complexes have large, multisubunit structures, and Complex IV is an example. It has a molecular mass of 204 kDa, contains 13 subunits, and has several redox centers, making its mechanism difficult to elucidate. High-resolution structures of Complex IV have been published,[73–75] enabling theoretical studies to probe the coupled ET/PT mechanism of this complex. The author of this analysis postulates that Complex IV couples electron tunneling between redox centers with a proton moving along a conduction channel in a "classical, diffusion-like random walk fashion,"[72] but concludes that much more work is needed to fully understand the coupled ET/PT reactions occurring in the ETC.

2.1.4 Mechanosensitive Ion Channels

Mechanosensitive ion channels (MSCs) are transmembrane proteins that are important in helping cells respond to a variety of mechanical stimuli, such as sound, gravity, and osmotic pressure gradients. They are found in a variety of tissues and are thought to be important for the senses of touch, hearing, and balance.[76] It currently is believed that two types of MSCs exist. The first type is found in specialized sensory cells; forces are applied to these channels through fibrous proteins.[77,78] The second type responds to stresses in the lipid bilayer.[77,79,80] The lipid membrane is often what the initial stress acts upon, and the lipid bilayer must somehow respond to these stimuli (see Chapter 1). A known function of MSCs includes regulating cell volume in response to osmotic pressure gradients, to prevent the cell from bursting. Somehow these transmembrane channels must detect extracellular forces, and transmit the information inside the cell as electrical or chemical signals.[81]

2.1.4.1 Gate Mechanisms

A defining characteristic of MSCs represents large conformational changes between the open and closed forms. For example, the bacterial large conductance mechanosensitive (MscL) channel undergoes a radius change of 5–6 nm between the open and closed forms.[82] An initial descriptor of the energy difference, ΔG, between open and closed forms based on the bilayer tension, T, is given by

$$\Delta G = T \times \Delta A, \qquad (2.14)$$

where ΔA is the in-plane area change between open and closed states.[77,83] However, there are likely more conformational changes, or deformations, possible for these MSCs, as the in-plane area does not take account of other channel conformational changes (see below), membrane stiffness, and membrane thickness, all of which can affect channel opening and closing. It is believed that there are three types of changes that channels can undergo.[83] The first is as mentioned above, where a channel can change its in-plane area, A. The second type occurs when a channel actually changes its shape within the membrane. Finally, a channel can also undergo a change in length without changing its shape or in-plane area. See Figure 1 in Markin and Sachs[83] for a nice illustration of the three types of conformational changes.

This system presents another situation where modeling studies can complement experimental studies. In the last several years there have been a few computational studies that look at gating mechanisms using a variety of models.[84–87] A recent computational study of the *Escherichia coli* MscL channel investigated the gating pathways when various conformational deformations are simulated.[87] It is known that, in general, the channel protein and the membrane undergo a deformation leading to the opening of the channel, but a molecular understanding of the process has not yet been achieved. The authors of the recent computational study examined the mechanical roles of structural features, such as transmembrane helices and loops, and found that many of these strongly affect gating ability. However, many questions remain in the drive to understand these interesting and complex channels on a molecular level.

References

1. Sharp, K. A. and Honig, B., Electrostatic interactions in macromolecules: Theory and applications, *Annu. Rev. Biophys. Biophys. Chem.* 1990, 19, 301–332.
2. Perutz, M. F., Electrostatic effects in proteins, *Science* 1978, 4362, 1187–1191.
3. Hol, W. G. J., The role of the α-helix dipole in protein structure and function, *Prog. Biophys. Mol. Biol.* 1985, 45 (3), 149–195.
4. Warshel, A., Energetics of enzyme catalysis, *Proc. Natl. Acad. Sci. U.S.A.* 1978, 75 (11), 5250–5254.
5. Braun-Sand, S. and Warshel, A., *Protein Folding Handbook*. 2005, 1, 163–200, Wiley, Hoboken, NJ.
6. Tanford, C., J. Theory of protein titration curves. II. Calculations for simple models at low ionic strength, *Am. Chem. Soc.* 1957, 79, 5340–5347.
7. Warshel, A., Russell, S. T., and Churg, A. K., Macroscopic models for studies of electrostatic interactions in proteins: Limitations and applicability, *Proc. Natl. Acad. Sci. U.S.A.* 1984, 81 (15), 4785–4789.
8. Georgescu, R. E., Alexov, E. G., and Gunner, M. R., Combining conformational flexibility and continuum electrostatics for calculating pKa's in proteins, *Biophys. J* 2002, 83 (4), 1731–1748.
9. Warwicker, J. and Watson, H. C., Calculation of the electric potential in the active site cleft due to alpha-helix dipoles, *J Mol. Biol.* 1982, 157 (4), 671–679.
10. Lee, F. S., Chu, Z. T., Bolger, M. B., and Warshel, A., Calculations of antibody-antigen interactions: Microscopic and semi-microscopic evaluation of the free energies of binding of phosphorylcholine analogs to McPC603, *Protein Eng.* 1992, 5 (3), 215–228.
11. Warshel, A., Sussman, F., and King, G., Free energy of charges in solvated proteins: Microscopic calculations using a reversible charging process, *Biochemistry* 1986, 25 (26), 8368–8372.
12. Klamt, A., Mennucci, B., Tomasi, J., Barone, V., Curutchet, C., Orozco, M., and Luque, F. J., On the performance of continuum solvation methods. A comment on "Universal Approaches to Solvation Modeling," *Acc. Chem. Res.* 2009, 42 (4), 489–492.
13. Hummer, G., Pratt, L. R., and Garcia, A. F., On the free energy of ionic hydration, *J Phys. Chem.* 1996, 100 (4), 1206–1215.
14. Ha-Duong, T., Phan, S., Marchi, M., and Borgis, D., Electrostatics on particles: Phenomenological and orientational density functional theory approach, *J Chem. Phys.* 2002, 117 (2), 541–556.
15. Parson, W. W. and Warshel, A., 2008. Calculations of electrostatic energies in proteins using microscopic, semi-microscopic and macroscopic models and free-energy perturbation approaches. In: Aartsma, T. J. and Matysik, J. (eds), *Biophysical Techniques in Photosynthesis,* vol 2, Series Advances in Photosynthesis and Respiration, vol 26. Springer, Dordrecht, pp. 401–420.
16. Molaris Manual and User Guide, 2009 (Theoretical Background). USC: Los Angeles, CA, 2009. http://laetro.usc.edu/programs/doc/molaris_manual.pdf
17. Warshel, A. and Russell, S. T., Calculations of electrostatic interactions in biological systems and in solutions, *Q. Rev. Biophys.* 1984, 17 (3), 283–422.
18. Lee, F. S., Chu, Z. T., and Warshel, A., Microscopic and semi-microscopic calculations of electrostatic energies in proteins by the POLARIS and Enzymix programs, *J Comput. Chem.* 1993, 14 (2), 161–185.
19. Warshel, A., Naray-Szabo, G., Sussman, F., and Hwang, J. K., How do serine proteases really work?, *Biochemistry* 1989, 28 (9), 3629–3637.
20. De Pelichy, L. D. G., Eidsness, M. K., Kurtz, D. M., Jr., Scott, R. A., and Smith, E. T., Pressure-controlled voltammetry of a redox protein: An experimental approach to probing the internal protein dielectric constant?, *Curr. Sep.* 1998, 17 (3), 79–82.
21. Schutz, C. N. and Warshel, A., What are the dielectric "constants" of proteins and how to validate electrostatic models?, *Proteins: Struct., Funct., Genet.* 2001, 44 (4), 400–417.
22. Ng Jin, A., Vora, T., Krishnamurthy, V., and Chung, S.-H., Estimating the dielectric constant of the channel protein and pore, *Eur. Biophys. J.* 2008, 37 (2), 213–222.

23. Burykin, A., Kato, M., and Warshel, A., Exploring the origin of the ion selectivity of the KcsA potassium channel, *Proteins: Struct., Funct., Genet.* 2003, 52 (3), 412–426.
24. LeMasurier, M., Heginbotham, L., and Miller, C., KcsA: it's a potassium channel, *J Gen. Physiol.* 2001, 118 (3), 303–313.
25. Cuello, L. G., Romero, J. G., Cortes, D. M., and Perozo, E., pH-dependent gating in the Streptomyces lividans K+ channel, *Biochemistry* 1998, 37 (10), 3229–3236.
26. Zhou, Y., Morals-Cabral, J. H., Kaufman, A., and MacKinnon, R., Chemistry of ion coordination and hydration revealed by a K+ channel-Fab complex at 2.0 A resolution, *Nature* 2001, 414 (6859), 43–48.
27. Doyle, D. A., Cabral, J. M., Pfuetzner, R. A., Kuo, A., Gulbis, J. M., Cohen, S. L., Chait, B. T., and MacKinnon, R., The structure of the potassium channel: molecular basis of K+ conduction and selectivity, *Science* 1998, 280 (5360), 69–77.
28. Aqvist, J. and Luzhkov, V., Ion permeation mechanism of the potassium channel, *Nature* 2000, 404 (6780), 881–884.
29. Luzhkov, V. B. and Aqvist, J., K+/Na+ selectivity of the KcsA potassium channel from microscopic free energy perturbation calculations, *Biochim. Biophys. Acta, Protein Struct. Mol. Enzymol.* 2001, 1548 (2), 194–202.
30. Allen, T. W., Bliznyuk, A., Rendell, A. P., Kuyucak, S., and Chung, S. H., Molecular Dynamics Estimates of Ion Diffusion in Model Hydrophobic and the KcsA Potassium Channel, *J Chem. Phys.* 2000, 112 (18), 8191–8204.
31. Allen, T. W., Hoyles, M., Kuyucak, S., and Chung, S. H., Molecular and Brownian dynamics studies of the potassium channel, *Chem. Phys. Lett.* 1999, 313 (1,2), 358–365.
32. Berneche, S. and Roux, B., Energetics of ion conduction through the K+ channel, *Nature (London)* 2001, 414 (6859), 73–77.
33. Biggin, P. C., Smith, G. R., Shrivastava, I., Choe, S., and Sansom, M. S. P., Potassium and sodium ions in a potassium channel studied by molecular dynamics simulations, *Biochim. Biophys. Acta, Biomembr.* 2001, 1510 (1–2), 1–9.
34. Warshel, A. and Weiss, R. M., An empirical valence bond approach for comparing reactions in solutions and in enzymes, *J. Am. Chem. Soc.* 1980, 102 (20), 6218–6226.
35. Warshel, A., *Computer modeling of Chemical Reactions in Enzymes and Solutions.* Wiley: New York, 1991.
36. Lanyi, J. K., Bacteriorhodopsin, *Annu. Rev. Physiol.* 2004, 66, 665–688.
37. Wikstrom, M. K. F., Proton pump coupled to cytochrome c oxidase in mitochondria, *Nature* 1977, 266 (5599), 271–273.
38. Warshel, A., Electrostatic basis of structure-function correlation in protein, *Acc. Chem. Res.* 1981, 14 (9), 284–290.
39. Mitchell, P., Coupling of phosphorylation to electron and hydrogen transfer by a chemi-osmotic type of mechanism, *Nature* 1961, 191, 144–148.
40. Mathies, R. A., Lin, S. W., Ames, J. B., and Pollard, W. T., From femtoseconds to biology: Mechanism of bacteriorhodopsin's light-driven proton pump, *Annu. Rev. Biophys. Biophys. Chem.* 1991, 20, 491–518.
41. Subramaniam, S. and Henderson, R., Molecular mechanism of vectorial proton translocation by bacteriorhodopsin, *Nature* 2000, 406 (6796), 653–657.
42. Henderson, R., The purple membrane from Halobacterium halobium, *Annu. Rev. Biophys. Bioeng.* 1977, 6, 87–109.
43. Oesterhelt, D. and Tittor, J., Two pumps, one principle: Light-driven ion transport in halobacteria, *Trends Biochem. Sci.* 1989, 14 (2), 57–61.
44. Michel, H., Behr, J., Harrenga, A., and Kannt, A., Cytochrome *c*-oxidase: Structure and spectroscopy, *Annu. Rev. Biophys. Biomol. Struct.* 1998, 27, 329–356.
45. Stoeckenius, W. and Bogomolni, R. A., Bacteriorhodopsin and related pigments of halobacteria, *Annu. Rev. Biochem.* 1982, 51, 587–616.
46. Warshel, A. and Parson, W. W., Dynamics of biochemical and biophysical reactions: insight from computer simulations, *Q. Rev. Biophys.* 2001, 34 (4), 563–679.
47. Braun-Sand, S., Sharma, P. K., Chu, Z. T., Pisliakov, A. V., and Warshel, A., The energetics of the primary proton transfer in bacteriorhodopsin revisited: It is a sequential light-induced charge separation after all, *Biochim. Biophys. Acta, Bioenerg.* 2008, 1777 (5), 441–452.
48. Luecke, H., Atomic resolution structures of bacteriorhodopsin photocycle intermediates: the role of discrete water molecules in the function of this light-driven ion pump, *Biochim. Biophys. Acta, Bioenerg.* 2000, 1460 (1), 133–156.
49. Herzfeld, J. and Lansing, J. C., Magnetic resonance studies of the bacteriorhodopsin pump cycle, *Annu. Rev. Biophys. Biomol. Struct.* 2002, 31, 73–95.
50. Royant, A., Edman, K., Ursby, T., Pebay-Peyroula, E., Landau, E. M., and Neutze, R., Helix deformation is coupled to vectorial proton transport in the photocycle of bacteriorhodopsin, *Nature* 2000, 406 (6796), 645–648.
51. Song, Y., Mao, J., and Gunner, M. R., Calculation of proton transfers in bacteriorhodopsin bR and M intermediates, *Biochemistry* 2003, 42 (33), 9875–9888.
52. Spassov, V. Z., Luecke, H., Gerwert, K., and Bashford, D., pK_a calculations suggest storage of an excess proton in a hydrogen-bonded water network in Bacteriorhodopsin, *J Mol. Biol.* 2001, 312 (1), 203–219.
53. Sampogna, R. V. and Honig, B., Environmental effects on the protonation states of active site residues in bacteriorhodopsin, *Biophys. J* 1994, 66 (5), 1341–1352.
54. Warshel, A., Conversion of light energy to electrostatic energy in the proton pump of *Halobacterium halobium*, *Photochem. Photobiol.* 1979, 30 (2), 285–290.
55. Lanyi, J. K., X-ray diffraction of bacteriorhodopsin photocycle intermediates, *Mol. Membr. Biol.* 2004, 21 (3), 143–150.
56. Warshel, A., Semiempirical methods of electronic structure calculation. In: G. A. Segal (Ed.) *Modern Theoretical Chemistry*, Vol. 7, Part A, p. 133, 1977, Plenum Press: New York.
57. Mitchell, P. and Moyle, J., Chemiosmotic hypothesis of oxidative phosphorylation, *Nature* 1967, 213 (5072), 137–139.

58. Jeremy, M. Berg, J. L. T., and Lubert S., *Biochemistry*. Sixth edition, W. H. Freeman and Company, New York, 2006.
59. Bollinger, J. M., Jr., Biochemistry. Electron relay in proteins, *Science* 2008, 320 (5884), 1730–1731.
60. Hurley, J. K., Tollin, G., Medina, M., and Gomez-Moreno, C., Electron transfer from ferredoxin and flavodoxin to ferredoxin-NADP+ reductase, In: Golbeck, J. H. (Ed.), *Photosystem I, the Light-Driven Plastocyanin:Ferredoxin Oxireductase*, pp. 455–476, 2006, Springer, Dordrecht.
61. Northrup, S. H., Kollipara, S., and Pathirathne, T., Simulation of rates of electron transfer between proteins cytochrome b5 reductase and cytochrome b5, *60th Southeast Regional Meeting of the American Chemical Society*, Nashville, TN, November 12–15 2008, SERM-098.
62. Shao, C., Zhao, C., Wang, Q., and Jiao, K., Direct electron transfer of redox proteins in sodium alginate solution, *Qingdao Keji, Daxue Xuebao (Ziran Kexueban)/ Journal of Qingdao University of Science and Technology* 2008, 29 (6), 474–479.
63. Brittain, T., Intra-molecular electron transfer in proteins, *Protein Pept. Lett.* 2008, 15 (6), 556–561.
64. Braun-Sand S., Olsson M. H. M., Mavri J., and Warshel A., Computer simulations of proton transfer in proteins and solutions, In: Hynes, J. T., Klinman, J. P., Limbach, H.-H., and Schowen, R. L. (Eds.), *Hydrogen Transfer Reactions*, 2007, Wiley-VCH, Hoboken, NJ.
65. Kandori, H., Yamazaki, Y., Sasaki, J., Needleman, R., Lanyi, J. K., and Maeda, A., Water-mediated proton transfer in proteins: An FTIR study of bacteriorhodopsin, *J Am. Chem. Soc.* 1995, 117 (7), 2118–2119.
66. Kim, S. Y. and Hammes-Schiffer, S., Hybrid quantum/classical molecular dynamics for a proton transfer reaction coupled to a dissipative bath, *J Chem. Phys*. 2006, 124 (24), 244102/1–244102/12.
67. Nie, B., Probing hydrogen bonding interactions and proton transfer in proteins. Oklahoma State University, Oklahoma, 2006. http://gradworks.umi.com/32/22/3222751.html
68. Gunner, M. R., Mao, J., Song, Y., and Kim, J., Factors influencing the energetics of electron and proton transfers in proteins. What can be learned from calculations, *Biochim. Biophys. Acta, Bioenerg.* 2006, 1757 (8), 942–968.
69. Camba, R., Jung, Y.-S., Hunsicker-Wang, L. M., Burgess, B. K., Stout, C. D., Hirst, J., and Armstrong, F. A., The role of the proximal proline in reactions of the [3Fe-4S] cluster in *Azotobacter vinelandii* ferredoxin I, *Biochemistry* 2003, 42 (36), 10589–10599.
70. Cukier, R. I. and Nocera, D. G., Proton-coupled electron transfer, *Annu. Rev. Phys. Chem.* 1998, 49, 337–369.
71. Hammes-Schiffer, S., Theoretical perspectives on proton-coupled electron transfer reactions, *Acc. Chem. Res.* 2001, 34 (4), 273–281.
72. Stuchebrukhov, A. A., Coupled electron and proton transfer reactions. Proton pumps, cytochrome oxidase, and biological energy transduction, *J Theor. Comput. Chem.* 2003, 2 (1), 91–118.
73. Yoshikawa, S., Shinzawa-itoh, K., Nakashima, R., Yaono, R., Yamashita, E., Inoue, N., Yao, M., et al., Redox-coupled crystal structural changes in bovine heart cytochrome *c*- oxidase, *Science* 1998, 280 (5370), 1723–1729.
74. Iwata, S., Ostermeier, C., Ludwig, B., and Michel, H., Structure at 2.8 Å resolution of cytochrome c oxidase from *Paracoccus denitrificans*, *Nature* 1995, 376 (6542), 660–669.
75. Abramson, J., Riistama, S., Larsson, G., Jasaitis, A., Svensson-Ek, M., Laakkonen, L., Puustinen, A., Iwata, S., and Wikstrom, M., The structure of the ubiquinol oxidase from Escherichia coli and its ubiquinone binding site, *Nat. Struct. Biol.* 2000, 7 (10), 910–917.
76. Pivetti, C. D., Yen, M.-R., Miller, S., Busch, W., Tseng, Y.-H., Booth, I. R., and Saier, M. H., Jr., Two families of mechanosensitive channel proteins, *Microbiol. Mol. Biol. Rev*. 2003, 67 (1), 66–85.
77. Gottlieb, P. A., Suchyna, T. M., Ostrow, L. W., and Sachs, F., Mechanosensitive ion channels as drug targets, *Curr. Drug Targets: CNS Neurol. Disord.* 2004, 3 (4), 287–295.
78. Ernstrom, G. G. and Chalfie, M., Genetics of sensory mechanotransduction, *Annu. Rev. Genet.* 2002, 36, 411–453.
79. Martinac, B. and Kloda, A., Evolutionary origins of mechanosensitive ion channels, *Prog. Biophys. Mol. Biol.* 2003, 82 (1–3), 11–24.
80. Sachs, F. and Morris, C. E., Mechanosensitive ion channels in nonspecialized cells, *Rev. Physiol., Biochem. Pharmacol.* 1998, 132, 1–77.
81. Martinac, B., Mechanosensitive ion channels: molecules of mechanotransduction, *J Cell Sci.* 2004, 117 (12), 2449–2460.
82. Chiang, C.-S., Anishkin, A., and Sukharev, S., Water dynamics and dewetting transitions in the small mechanosensitive channel MscS, *Biophys. J* 2004, 86 (5), 2846–2861.
83. Markin, V. S. and Sachs, F., Thermodynamics of mechanosensitivity, *Phys. Biol.* 2004, 1 (2), 110–124.
84. Sukharev, S., Durell, S. R., and Guy, H. R., Structural models of the MscL gating mechanism, *Biophys. J* 2001, 81 (2), 917–936.
85. Sukharev, S. and Anishkin, A., Mechanosensitive channels: What can we learn from 'simple' model systems?, *Trends Neurosci.* 2004, 27 (6), 345–351.
86. Gullingsrud, J. and Schulten, K., Gating of MscL studied by steered molecular dynamics, *Biophys. J* 2003, 85 (4), 2087–2099.
87. Tang, Y., Yoo, J., Yethiraj, A., Cui, Q., and Chen, X., Gating mechanisms of mechanosensitive channels of large conductance, II: Systematic study of conformational transitions., *Biophys. J* 2008, 95 (2), 581–596.

3

Cell Biology and Biophysics of the Cell Membrane

Didier Dréau

3.1 Cell Interactions

In contrast to unicellular organisms, in multicellular organisms cells interact with one another through cell–cell physical chemical (paracrine or hormonal) contacts. The physical cell–cell interactions occur through cell junctions with binding of proteins present within the membranes of each cell. For distant interactions, molecules secreted (ligands) are recognized by specific receptors on the target cell membrane or in the target cell, depending on the hydrophobicity of the ligand.

3.2 Types of Junctions

Three main types of cell–cell junctions define the physical strength of interactions between cells (Figure 3.1): desmosomes (zonulae adherens), tight junctions (zonulae occludens), and gap junctions. These junctions are cell membrane regions enriched with specific proteins interacting between two cells. In particular, the physical strength of the junction allows a resistance to shear stress (a stress applied parallel or tangential to a contact surface) imparted, for example, by vessel endothelium on blood or blood on vessel, respectively. The shear stress of a fluid or viscosity drag (t) is a function of its viscosity (η) and velocity (v) exerted on the wall of a lumen (inner radius r). Shear stress resistance characterizes the different cell junctions of a given lumen [e.g., blood vessels and the gastrointestinal (GI) tract]. The greater the viscosity [and the liquid flow (Q)], the higher the shear rate and the viscosity drag (t):

$$t = 4\eta Q / \pi r^3. \quad (3.1)$$

Note: In denominator $\pi = 3.1415926...$

3.2.1 Desmosomes

Desmosomes are found in all tissues subject to *shear stress*, including the skin and the GI tract. Desmosomes generate strong bonds between cells and between cells and the basal lamina. Proteins, mainly desmoglein and desmocollin, are associated in dense plaques, separated by a 30 nm intercellular space, are present in both cell membranes, and are linked to intracellular structures and tonofilaments in the two connected cells (Figure 3.1). Shear stress leads to deformation of the cell membrane and disruption of filament actin (F-actin) and of

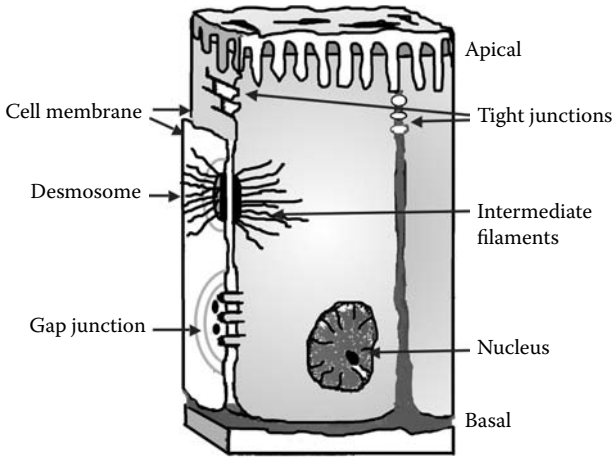

FIGURE 3.1 Type of cell junctions.

cytoskeleton organization. In response to disruption of F-actin, the expression of multiple proteins, including those involved in adherence and cell junctions, is up-regulated, depending on both type of cell and liquid flow. Hemidesmosomes are structures that are present on cells and use similar proteins to anchor cells to the basal lamina through interactions between integrins and proteins in the basal lamina.

3.2.2 Tight Junctions

Tight junctions are common in exchange tissues holding nephron cells in the kidneys, endothelial cells in the vessels, and enterocytes in the GI tract together. Tight junctions in cells are made through the interactions of multiple proteins, including claudins and occludins, both of which are transmembrane proteins embedded in the cytoskeleton. Tight junctions also prevent the movement of proteins with apical functions to the basolateral area of the cell membrane (and vice versa), ensuring cell polarity. Cell polarity also defines both chemical interactions and electrical gradients by the types and concentrations of receptors and channels present. As with chemical activity, cell membrane electrical potential can be different between the apical and the baso-lateral area of a cell.

3.2.3 Gap Junctions

Gap junctions are hemichannels or connexons composed of six connexin (Cx) proteins. The alignment of two connexons forms a gap junction between two cells, allowing cytoplasm sharing and the rapid transfer of both electrical and chemical signals (small molecules and ions). The type of connexins associated in the formation of the connexon (homo- and hetero-hexamers) appears to influence the function of the gap junctions (speed of electrical chemical transfers and nature of the chemical molecule transferred). The concentration of multiple (>100) gap junctions forms a complex structure or plaque. Gap junctions allow direct electrical signaling between cells, although differences (10- to 15-fold) in electrical conductance between gap junctions have been shown. Gap junctions also allow chemical molecules (<1000 Da) to move from one cell to the other and favor chemical communication through the passage of second messengers, including IP3 and Ca^{2+}. The passage of these chemicals is selective, depending on the size and charge of the molecule and the nature of connexin subunits. Although most of the movement of ions through gap junctions does not require energy, the recycling of K^+ in the cochlea, essential to the transduction by auditory hair cells through gap junctions, is facilitated by ATPase activity and connexin conformation changes.

Charge associated with the connexins either repulses or attracts ions, playing a critical role in preventing or allowing for passage. In addition to these chemical and electrical exchange functions, gap junction proteins also promote cell adhesion and have tumor suppressing (C×43, C×36) and cell signaling (C×43) roles. The presence of gap junctions linking multiple cells within a tissue generates a *syncytium*, that is, a duster of cells with similar response as in the heart muscle, and the smooth muscles of the GI tract.

3.3 Cell Adhesion Molecules

Within tissues, cells interact not only with other cells but also with the extracellular matrix (ECM). Cell attachment to the ECM is a key requirement of multicellular organisms. Produced by multiple cells, including fibroblasts, the ECM is composed of multiple proteins, of which the major ones are collagens, laminin, fibronectin, vitronectin, and vimentin. The ECM constitutes the basal lamina, the basal layer on which cells are anchored by integrins. These cell surface receptors are composed of one α (alpha) and one β (beta) subunit. Each heterodimer binds to a specific molecule of the ECM (e.g., $\alpha 6\beta 1$ binds to laminin) with variable affinities. Integrin expression is cell specific and the strength of the binding to the ECM is variable, depending on the composition of both integrin and ECM. The binding site for the ECM is on the β chain and requires divalent cations to function whereas the α subunit may be involved in protein stabilization.

Integrins attach cells to the ECM through interactions between ECM molecules and microfilaments of the actin cytoskeleton, allowing cells to resist shear stress forces. The intensity of the force needed to deform a cell membrane or dissociate a cell linked by junctions in an epithelium is highly variable and will depend on the force as well as on the characteristics of the specific location of interest.

This cell attachment involves not only integrins but also the formation of cell adhesion complexes consisting of transmembrane integrins and many cytoplasmic proteins, including talin, vinculin, and paxillin. Integrins have a prominent role in regulating cell shape, cell migration, and cell signaling, making them pivotal in multiple cell events (including growth, differentiation, and survival).

3.4 Intracellular Connections

Cell membranes are physically connected with the cellular scaffolding or cytoskeleton. The cytoskeleton, critical in cell shape

and motion, intracellular transport (vesicles and organelles), and cell division, is composed of three kinds of filaments: microfilaments, intermediate filaments, and microtubules. Microfilaments are intertwined double-helix actin chains that are concentrated near the cell membrane. Intermediate filaments are very stable and constituted of multiple proteins, including vimentin, keratin, and laminin. Microtubules are composed of tubulin (α and β), which play a major role in intracellular transport and in the formation of mitotic spindles. Connections of the membrane with the cytoskeleton are key in maintaining 3D structures, cell shape and deformation (e.g., generation of processes), and resistance to tension.

3.5 Cell Membranes and Epithelia

As for individual cells, where the membrane is a selective barrier allowing the movement of water and ions through channels and of larger molecules through specific carriers, the epithelium also benefits from the selective permeability of the cells itis made of. The movement of molecules through the semipermeable membrane that is the cell membrane or of cells lining an epithelium relies on various physiological mechanisms. The intrinsic permeability of the cell membrane depends on (1) the presence of a gradient, that is, a difference in the chemical concentration or electrical charge between both sides of the cell membrane, and (2) the movement of molecules through diffusion, leaky channels, or facilitated or active transport. The membrane transport processes are discussed in greater detail in the next section and will be referenced in Chapter 5 for the specific working action.

3.6 Membrane Permeability

3.6.1 Membrane Composition and Structure

Membranes are mostly made up of *hydrophobic* phospholipids (phosphatidylcholine, sphingomyelins, aminophospholipids, phosphatidylglycerol, and phosphatidylinositol), with one polar head and two nonpolar lipid chains. Hydrophobic means that the chemical structure is such that it repels the water dipole, in contrast to hydrophilic, which attracts water due to the inherent polar chemical composition. In an aqueous environment, the nonpolar chains are oriented away from water with the polar head in contact with the water, leading to the spontaneous formation of lipid bilayers. With the exception of the protein anchored internally to the actin or spectrin network or externally to ECM molecules, proteins can move within the lipid bilayer creating a fluid mosaic. The lipid:protein ratio can radically vary between membrane and cell types (Table 3.1).

Membrane composition is also heterogeneous, that is, protein distribution and, to a lesser extent, lipid composition are different throughout the cell membrane. Specifically, the density of a given receptor can be much higher at a specific location, for example, acetylcholine nicotinic receptors concentrated at the motor end plate. This cell polarity, defined by an asymmetry in the protein composition of the baso-lateral and apical membrane areas as delineated by thigh junctions, is critical in the development of epithelium and tissue whose major functions include exchanges.

TABLE 3.1 Cell Membrane Composition (%)

Membrane	Carbohydrate	Lipid	Protein
RBC 8		43	49
Myelin	3	79	18
Inner mitochondrial membrane	0	24	76

Source: Silverthorn D.U., *Human Physiology: An Integrated Approach*, 5th edition. Benjamin Cummings, San Francisco, CA, 2010.

The heterogeneous and asymmetric lipid bilayer forming the cell membrane through a constant and dynamic redistribution of proteins constitutes a *semipermeable barrier* separating two compartments with different chemical and ionic compositions. These differences in charges and concentrations associated with the asymmetrical membrane proteins generate *electrochemical gradients*, that is, differences in the net electrical charge and concentrations of a given solute inside versus outside the cell (Figure 3.2). Although both gradients are intertwined, each can act independently of the other.

3.6.2 Molecule Movements

Molecule movements between two compartments separated by a plasma membrane or an epithelium use *pericellular transport* (between cells), *transcellular transport* (through the membrane), and *endocytosis* and/or *exocytosis* mechanisms. In pericellular transport, molecules move through an epithelium using spaces between cells. During endocytosis and exocytosis, physical distortions of the cell membrane through vesicle creation or fusion allow the movement of molecules into or out of the cell without transport through the membrane (Figure 3.2).

Transcellular transport depends on multiple parameters, including the hydrophobicity of the molecule and the density of transport proteins. Small molecules use *diffusion* whereas larger molecules require specific *transport proteins*. The cell membrane is highly permeable to most *hydrophobic* molecules or lipid-soluble solutes such as alcohol, vitamins A and E, and steroids. In contrast, the *permeability of water-soluble* or *hydrophilic molecules* is limited to very *small molecules*, including water and hydrophobic molecules with specific carriers. Most membranes are impermeable to water-soluble molecules above 200 Da. Ions are relatively insoluble because of their charge in lipids; therefore, membranes are poorly permeable to ions. Ion diffusion occurs mostly through *ion channels*. Ion channels span the membrane and are specific to an ion or class of ions, mostly depending on size and charge. Amino acids and sugars also require specific *transporters* present in the cell membrane.

3.6.3 Diffusion

Small molecules, gases (O_2, CO_2, and NO), and molecules soluble in polar solvents diffuse through the cell membrane. *Diffusion* is driven by a gradient and continues until equilibrium. The net

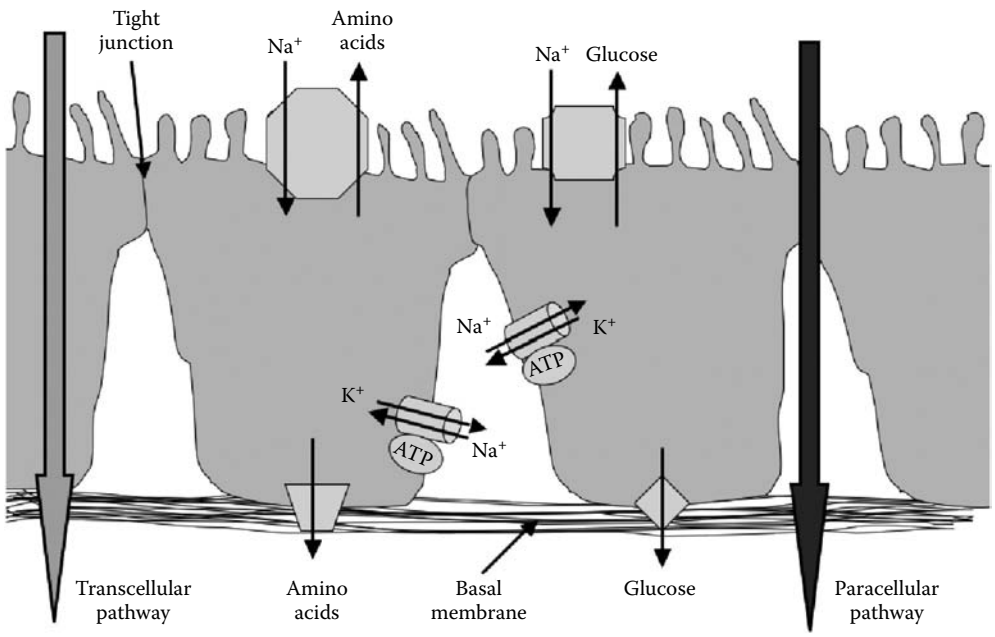

FIGURE 3.2 Transport through the cell membrane and epithelium.

diffusion rate (J) is proportional to the coefficient of diffusion (D), the surface area (A), the thickness of the membrane (Δx), and the gradient or difference in concentration (ΔC). The net diffusion rate is defined by Fick's law:

$$J = -DA\frac{\Delta C}{\Delta x}. \tag{3.2}$$

The *diffusion time* is a function of the thickness of the membrane and the permeability coefficient (Einstein relation). The diffusion time (t) is a function of average diffusion distance (Δx) and the coefficient of diffusion:

$$t = \frac{(\Delta x)^2}{2D}. \tag{3.3}$$

For small water-soluble molecules with a coefficient of diffusion equal to 10^{-5} cm^2/s, the diffusion times are 0.5 m, 50 m, 5 s, 8.3 min, and 14 h for membrane thicknesses of 1, 10, 100, 1000, and 10,000 μm, respectively. The diffusion time (Table 3.2) is proportional to the diffusion coefficient (D), which itself is proportional to the speed of movement of the molecule in a given medium: if the molecule is large and the medium is viscous, D is small.

For small molecules, D is inversely proportional to the molecular weight (MW) in dalton: $D = 1/\text{MW}$. For larger spherical molecules, the equation of Stokes–Einstein approximates the coefficient of diffusion (Equation 3.4), taking into account the gas constant (R), the absolute temperature (T), the number π, the Avogadro number (N), the solvent viscosity (η), and the radius of the molecule (r):

$$D = \frac{RT}{6N\pi r\eta} = 1.38 \times 10^{-23}\frac{T}{\pi r\eta}. \tag{3.4}$$

TABLE 3.2 Molecule Size, Coefficient, and Diffusion Time

Molecule	Radius (nm)	D	Time (s)
Oxygen 0.2		900	0.001
Sucrose	0.5	400	0.003
Insulin	1.4	160	0.01
Ribosome	10	22	0.06

3.6.4 Protein-Mediated Membrane Transport

Movements of large molecules require intrinsic specific *carriers* or *channels*. Through *conformational changes*, channels form gates, allowing the passage of molecules. Transporter recognition is ligand specific but generally not absolute, and related molecules can compete for or inhibit transport. These channels can be either *voltage gated* or *ligand gated*: the former is activated by difference in the transmembrane voltage difference and the latter by binding to its specific ligand.

Mediated membrane transport is more rapid than simple diffusion, can saturate, and is chemically specific and sensitive to competition. The transport rate (J) for a given molecule (S) is defined by its maximum transport rate (J_m), the Michaelis constant (K_m) and the concentration of the molecule ([S]), as described by the Michaelis–Menten equation:

$$J = \frac{J_m[\text{S}]}{K_m + [\text{S}]}. \tag{3.5}$$

The transport through a carrier is limited by the speed and capacity of each carrier with a conformational change of 10^3–10^4 solute molecules/s. For ion channels, through an open channel, ions move at 10^7–10^8 ions/s. In *facilitated transport*, no energy is involved, whereas *active transport* requires energy

(ATP mostly). Facilitated transport benefits from existing charge or concentration gradients to move molecules (e.g., GLU2 transporter and Na^+ gradients). Active transports promote the movement against concentration or electrochemical gradients using energy, mostly ATP, to cycle between its conformational states. For example, the Ca^{2+} ATPases move two Ca^{2+} from the lumen to the sarcoplasmic reticulum per ATP and the Na^+/K^+ ATPase, present in the plasma membrane of the cells, moves three Na^+ out of the cells and two K^+ into the cell per ATP. Because of the K^+ and Na^+ concentrations in and out of the cells, these tend to move passively toward equilibrium, and the steady state for these ions is maintained by the constant activity of the Na^+/K^+ ATPases.

3.7 Osmotic Pressure and Cell Volume

The cell volume is directly related to the internal pressure, and hence the osmotic pressure is also affected by the cell volume.

3.7.1 Osmotic Pressure

Osmosis is defined as the flow of water across a semipermeable membrane (i.e., permeable to water only) from a compartment with a low solute concentration to a compartment with a high solute concentration. *Osmotic pressure* is the pressure that is sufficient to prevent water from entering the cell. Osmotic pressure (Π) is directly associated with the number of ions formed from the dissociation of a solute (i), the molar concentration of the solute (c), and the osmotic coefficient (ϕ) and can be calculated by van't Hoff's law:

$$\Pi = RT(i\phi c). \quad (3.6)$$

Osmotic pressure is a function of the concentration of solute present on either side of the membrane, and the concentration of solute also increases the boiling point and lowers the freezing point. Osmotic pressure (Π) is a function of the concentration of solute present on either side of the membrane. Since the concentration of solute is proportional to the solute freezing point, the osmotic pressure can also be estimated based on the freezing point depression (ΔT_f):

$$\Pi = RT(\Delta T_f/1.86). \quad (3.7)$$

where ΔT_f is the freezing point depression. Two solutions separated by a semipermeable membrane are *isoosmotic* (have equal osmotic pressures), *hyperosmotic* (A hyperosmotic compared to B), or *hypoosmotic* (B compared to A). Osmotic coefficients have been calculated (Table 3.3).

3.8 Tonicity

The plasma membrane of animal cells is relatively impermeable to many solutes but highly permeable to water. Therefore, increase in the osmotic pressure of the extracellular fluid (ECF) leads to water leaving the cells through osmosis, resulting in cell shrinking. In contrast, if the ECF is diluted, water enters the cells, resulting in cell swelling. Swelling activates channels, increasing efflux of K^+, Cl^-, and the water that follows by osmosis returns cells to normal size. Both cell shrinking and swelling will continue until the osmotic pressures on both sides are equal or *isoosmotic*.

TABLE 3.3 Osmotic Coefficients

Compound	i	MW (Da)	ϕ
NaCl	2	58.3	0.93
KCl	2	74.6	0.92
HCl	2	36.6	0.95
$CaCl_2$	3	111.0	0.86
$MgCl_2$	3	95.2	0.89
Glucose	1	180.0	1.01
Lactose	1	342.0	1.01

Source: Lifson N. and Visscher M.B., In O. Glasser (Ed.), *Medical Physics*, Vol. 1, St. Louis, MO, 1944.

In vivo, protein concentration is the most important parameter generating oncotic pressure, which contributes to the net flow of a given solute. Both the shrinking and swelling drastically impair cell function and potentially, in extreme cases, its survival. In living organisms, cells are suspended in a mixture of *permeant* and nonpermeant solutes. In those conditions (1) the steady volume of a cell is determined by the concentration of nonpermeant solutes in the ECF, (2) permeant solutes generate only transient alterations of the cell volume, and (3) the greater the cell permeability to a permeant solute, the faster the time course to transient change.

3.9 Electrical Properties of Cell Membranes

The electrical properties of the cell membrane are derived from their insulator potential associated with the composition, especially the amount of lipid present. For example, myelin produced by Schwann cells leads to the insulation of axons, with multiple layers of the cell membrane preventing loss of electrical charges. The electrical properties of the cells are also a function of the constantly maintained disequilibrium of the ions generated by the tight control of ion movements and charges present on either side of the membrane. Additionally, cell transport through channels for ions or carriers for proteins also affects the electrical charges present on each side of the cell membrane, leading to alterations in the local membrane potential.

3.9.1 Forces Acting on Ion Movements

Several forces act on the components surrounding the membrane. The two main categories are electrical forces and chemical gradient forces.

In living animal cells, a comparison of the composition of the cytosol and the ECF underlines the presence of proteins

(generally negatively charged) and K^+ at high concentrations inside the cell, whereas Ca^{2+}, Na^+, and Cl^- concentrations are higher in the ECF. *Permeant* molecules, including some ions, move continuously in or out of the cell through leaky *channels* of the cell membrane following electrical and chemical gradients. The difference in charge between the inside and outside of a cell creates a *membrane potential* or the amount of energy (electrical) associated with the electrochemical gradient present. The net gradient for a given ion and cell remains stable because ATP-dependent ion pumps, especially the Na^+/K^+ ATPase, continuously and actively maintain these equilibriums.

3.9.2 Distribution of Permeable Ions

Taking into account the ions that cannot diffuse, the distribution of permeable ions is predicted by the Donnan–Gibbs equilibrium: in the presence of a nondiffusible ion (e.g., protein), a diffusible pair of ions of the same valence distributes to generate equal concentration ratios, for example,

$$[K^+]_{in} \times [Cl^-]_{in} = [K^+]_{out} \times [Cl^-]_{out}. \quad (3.8)$$

The overall membrane potential at any time is a function of the distribution (inside versus outside) and membrane permeability to Na^+, K^+, and Cl^- (Figure 3.3).

The Donnan–Gibbs equilibrium explains the critical role of the Na^+/K^+ ATPase pump in constantly removing Na^+ ions out of the cells to maintain osmotic pressure and cell volume. It also clarifies the electrical difference generated by the asymmetric distribution of permeable ions between the intracellular and extracellular compartments at equilibrium. Along the membrane on the extracellular side, the charges created by Cl^- are balanced by the K^+ ions that are present inside the cell. This effect is also critical in the movement of ions across the capillary wall mostly generated by the higher protein concentration in the plasma compared to the ECF.

3.9.3 Membrane Potential

The relationship between the chemical and electrical forces acting on ions across the plasma membrane and the generation of the resting membrane potential is defined by taking into account the ion valence (Z_{ion}) and ECF ($[ion]_{out}$) and (intracellular fluid) ICF ($[ion]_{in}$) concentrations as described in the Nernst equation:

$$E_{ion} = \frac{RT}{FZ_{ion}} \log_{10}\left(\frac{[ion]_{out}}{[ion]_{in}}\right), \quad (3.9)$$

where R is the gas constant, F is the Faraday constant, and T is the absolute temperature. At 37°C, the equation can be simplified to $E_{ion} = 61.5 \log_{10}([ion]_{out}/[ion]_{in})$. For Cl^-, with intra- and extracellular Cl^- concentrations of 9.0 and 125.0 mM, $E_{Cl-} = -70$ mV, a value identical to the one measured experimentally. In neurons, calculated E_K^+ (–90 mV) differs from measured E_K^+ (–70 mV). Similarly, the difference between calculated E_{Na}^+

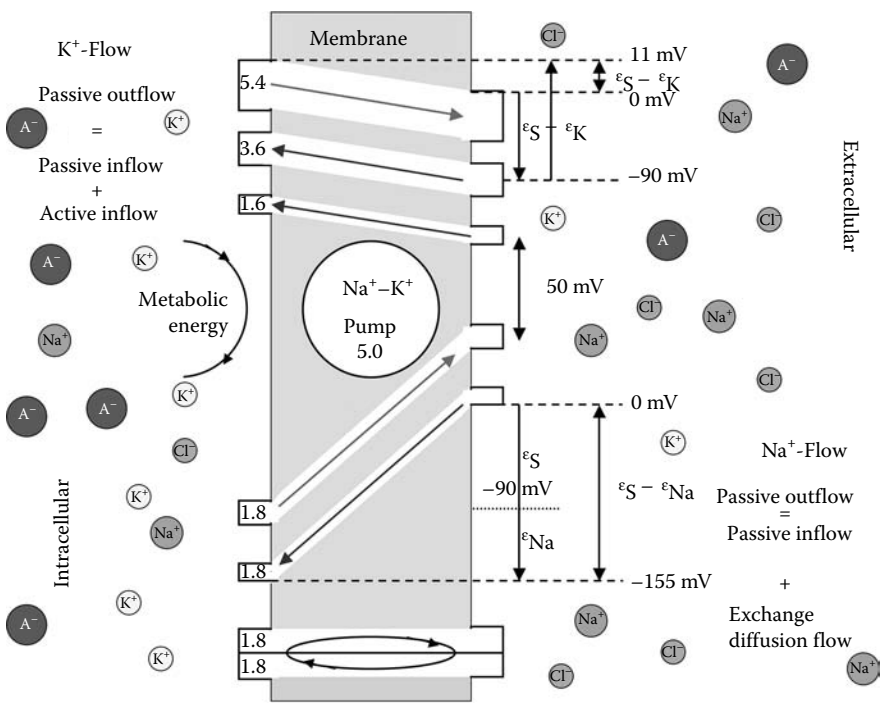

FIGURE 3.3 Ion exchanges and the creation of an electrochemical gradient across the cell membrane. The influence of protein (A^-), Cl^-, K^+, and Na^+ extracellular and intracellular concentrations and the role of Na^+/K^+ ATPase active transport roles in the generation of the electrochemical gradient are represented.

(+60 mV) and measured E^{+}_{Na} suggests that other ions may play a role in the equilibrium potential in those cells. These differences from the optimal membrane potentials of each of these ions are actively maintained through the action of the Na^+/K^+ ATPases pumping three Na^+ out and two K^+ per ATP molecule.

The K^+ efflux is counterbalanced by the electrical gradient of more negative charges (the bulk of which are proteins) inside the cell. The constant activities of the Na^+/K^+ ATPases pumping K^+ inside and removing Na^+ prevent these ions from reaching the equilibrium associated with their respective electrochemical gradients.

3.10 ATPases

ATPases are evolutionary conserved proteins with three major types: P, V, and F. The P type involves a phosphorylated intermediate and includes Na^+/K^+ ATPases and Ca^{2+} ATPases. Mostly present on cell organelles (storage granules and lysosomes), the V type accumulates H^+ in vesicle lumen. Most cell membranes also contain Na^+/H^+ exchangers to prevent the acidification of the cytosol becoming active when the pH of the cytosol decreases, with Na^+ moving following its electrochemical gradient in exchange with the movement of H^+ out of the cell.

In contrast to P and V ATPases, which consume ATP, the F type represented by ATP synthase of the inner mitochondrial membrane is a major source of ATP. ATP production depends on the oxygen conditions. In anaerobic conditions, one glucose molecule produces two pyruvate molecules transformed in lactate, yielding a net energy of two ATPs. In aerobic conditions, pyruvate molecules enter the citric acid cycle in the mitochondria and through oxidative phosphorylation yield up to 30–32 ATP molecules.

3.10.1 Role of ATPases

In excitable cells, following an action potential in which Na^+ and K^+ ions move in and out of the cell respectively, the cell repolarizes with an efflux of K^+ ions. K^+ channels are slow to close and the K^+ efflux generates a hyperpolarization of the cell membrane. The equilibrium is re-established by the activity of the sodium/potassium ATPase pump moving three Na^+ ions out and allowing two K^+ ions in through active transport through a conformational change.

The efflux of Na^+ provides the driving force for multiple facilitated transport mechanisms, including glucose, amino acid membrane transport, and creates an osmotic gradient that promotes the absorption of water. In the enterocytes of the GI tract, on the baso-lateral surface of the cell, Na^+ is pumped out of the cell through the activity of Na^+–K^+ ATPase pumps creating a gradient that favors the influx of Na^+ from the apical side of the cell.

3.10.2 Regulation of Na^+/K^+ ATPase Activity

The activity of the ATPase pump is endogenously down-regulated through increases in cyclic adenosine monophosphate (cAMP) associated with G protein coupled receptor activations and up-regulated through decreases in cAMP by ligands leading to G protein coupled receptor inhibition. Thyroid hormones, insulin, and aldosterone increase the expression of Na^+/K^+ ATPase pumps and therefore the activity. In contrast, in the kidney, dopamine induces the phosphorylation of the Na^+/K^+ ATPase pump, inhibiting its activity.

3.11 Cell Membrane and pH Regulation

Mechanisms in cells allow the regulation of H^+ intracytoplasmic concentrations including through the activity of the Na^+/H^+ ATPase, which prevents H^+ increases into the cytosol by pumping H^+ in specific cell compartments. Intracellular H^+ concentration is influenced by ECF and plasma H^+ concentration.

In the plasma, the H^+ concentration is very low compared to other ions (~0.0004 mEq/L) and is expressed as the negative log of the H^+ concentration (or pH). The plasma pH ranges from 7.38 to 7.42, with extreme acidosis at 7.0 and extreme alkalosis at 7.7. Throughout the body, pH values are very variable with, for example, gastric HCl (0.8), urine (as low as 4.5), and pancreatic juice (8.0). Because pH homeostasis is essential to organism survival through enzymatic and membrane and capillary exchanges, the pH is tightly monitored through central and peripheral sensors and regulated by buffers, the lung, and kidney activities. Like other chemicals, the organism has sensing mechanisms with properties comparable to those observed in smell and taste senses, including pH sensors, and a constant feedback regulation and monitoring of the ECF and plasma pH.

3.11.1 pH Sensors

Chemoreceptors sensing H^+ concentrations in the plasma and cerebrospinal fluid, respectively, are located peripherally in the aortic arch (aortic bodies) and at the bifurcation of the internal and external carotid in the neck (carotid bodies) and centrally in the brain medulla. The blood–brain barrier is poorly permeable to H^+ but allows CO_2 diffusion. The addition of CO_2 displaces the equilibrium bicarbonate hydrogen toward the formation of more H^+, increasing the pH of the cerebrospinal fluid (CSF):

$$CO_2 + H_2O \Leftrightarrow H_2CO_3 \Leftrightarrow H^+ + HCO_3^-. \qquad (3.10)$$

This decrease in pH is sensed by chemoreceptors that stimulate lung ventilation to bring H^+ and CO_2 concentrations within range.

3.11.2 pH Regulation

In mammalians, pH regulation is achieved through (1) buffers and the activities of (2) the lung and to a lesser extent (3) the kidneys. Buffers are molecules that combine with H^+, neutralizing its effects. The presence of buffers moderates greatly the addition of H^+ to a solution. Buffers such as $H_2PO_4^{2-}$ and HCO_3^- are present in cells and ECF, respectively. Also, an increase in

plasma CO_2 is associated with an increase in H^+ in the CSF sensed in the medulla, leading to a rapid increase in lung ventilation to remove CO_2 and maintain ECF pH. If despite buffer effects and ventilation modulations, pH acidification or alkalination persist, the kidney can secrete or absorb H^+ ion and HCO_3^- ion. Following conversion of CO_2 into HCO_3^- by carbonic anhydrase in proximal tubule cells, HCO_3^- is reabsorbed and H^+ is secreted. Alternatively, H^+ is secreted as ammonium ion NH^{4+}. In the distal nephron, intercalated cells or either type A or B functioning during acidosis or alkalosis excrete H^+ or HCO_3^- and K^+, respectively (see Equation 3.10).

3.11.3 Gas Exchanges and pH Regulation

Cells of the organism receive signaling molecules, nutrients, and O_2 through the cardiovascular system and the ECF. As described above, removal of CO_2 produced by cellular metabolism is critical to the maintenance of a pH compatible with normal cell function. CO_2 is carried in the blood as (about 70%) bicarbonate ions HCO_3^- (see Equation 3.10) by a carbonic anhydrase in the red blood cells (RBCs), 7% is dissolved in the plasma, and 23% is bound to hemoglobin at a site other than O_2. The binding to CO_2, however, decreases hemoglobin O_2 binding, in effect allowing more O_2 release in a region with high CO_2 concentrations. This effect (Bohr effect) is observed when increases in the partial pressure of CO_2 or lower pH values result in the off-loading of oxygen from hemoglobin.

3.12 Summary

In multicellular organisms, cell interactions depending on cell junctions and adhesions to the ECM modulate individual cell function and epithelium membrane permeability. In addition to diffusion, molecules are transported through protein carriers with or without energy requirements. The chemical and electrical inbalance between compartments separated by the lipid bilayer cell membrane is actively maintained by ATPases. These electrical and chemical disequilibria generate electrochemical gradients and the membrane potential critical in cell functions.

Additional Reading

1. Yeagle P.L., *The Structure of Biological Membranes*, 2nd edition. CRC, Boca Raton, FL, 2004.
2. Alberts B., Johnson A., Lewis J., Raff M., Roberts K., and Walter P., *Molecular Biology of the Cell*, 5th edition. Garland Science, Oxford, UK, 2008.
3. Landowne D., *Cell Physiology*, 1st edition. McGraw-Hill Medical, New York, NY, 2006.
4. Ethier C.R. and Simmons C.A., *Introductory Biomechanics: From Cells to Organisms*, 1st edition. Cambridge Texts in Biomedical Engineering, New York, NY, 2007.
5. Barrett K.E., Brooks H., Boitano S., and Barman S.M., *Ganong's Review of Medical Physiology*, 23rd edition. McGraw-Hill Medical, New York, NY, 2009.
6. Silverthorn D.U., *Human Physiology: An Integrated Approach*, 5th edition. Benjamin Cummings, San Francisco, CA, 2010.
7. Koeppen B.M. and Stanton B.M., *Berne and Levy Physiology*, 6th edition. St. Louis, MO, 2008.
8. Lang F., Vallon V., Knipper M., and Wangemann P., Functional significance of channels and transporters expressed in the inner ear and kidney. *Am. J. Physiol. Cell Physiol.*, 293: C1187–208, 2007.
9. Lifson N. and Visscher M.B., Osmosis in living systems in O. Glasser (Ed.), *Medical Physics*, Vol. 1, St. Louis, MO, 1944.

4

Cellular Thermodynamics

Pavlina Pike

4.1 Introduction

Every living organism is built with a network of billions of cells, which communicate among each other and with the surroundings by the controlled exchange of chemical and electrical signals. These signals are molecules and ions that carry information used by the cells to perform certain tasks, such as the activation of enzymes or genes, cellular proliferation, and death. A major role in this exchange is played by the cell membrane and more specifically by structures called ion channels and gap junctions. The purpose of this paragraph is to introduce ion transport in cells from the point of view of thermodynamics. We will start with the basic terms and laws that are the building blocks of thermodynamics. Attention will be given to excitable cells, that is, cells that respond to electrical signals, especially heart muscle cells.

4.2 Energy

Energy is needed to sustain life in all its forms. The most powerful natural source of energy for the Earth is the Sun. The amount of energy that reaches the Earth is 1366 W/m^2, which includes light of all wavelengths irradiated by the Sun.[1] This energy is used in every aspect of life to sustain it. For example, visible light is essential in photosynthesis in plants, activation of photosensitive cells in the eye, regulation of the circadian cycle by the hypothalamus, etc. Energy is also used for electrical signal conduction and neurotransmitter release in nerve cells: importing/exporting and processing ions and molecules in cells. Energy is stored in cells (potential energy) in the form of bonds between the phosphate groups in the adenosine triphosphate (ATP) molecule. If one of these bonds is broken, energy is released and then used for different endergonic (energy gaining) reactions in the cell. But what is energy? So far there is no clear definition. *Energy* is most commonly defined as the ability of an object to do work. It can be either supplied or taken away from the system in order for the processes (changes) to occur. The energy transfer to or from the system is called *work*.

The sum of the kinetic, potential, chemical, nuclear, and so on energies of particles in a system is called the *internal energy* (U) of a system. For simplicity, we will consider the internal energy to only consist of the potential energy of molecular bonds and the kinetic energy of the microscopic motion of atoms. It is also described as the energy that is required for the system to be created assuming constant temperature and volume.

The laws that govern energy transfer, or the conversion of energy from one form to another, are described by thermodynamics.

4.3 Laws of Thermodynamics

4.3.1 The First Law of Thermodynamics

The first law of thermodynamics states that the change in the internal energy of a system is the net result of the heat (Q) added to the system and the work (W) done by the system on the surroundings, as given by Equation 4.1:

$$\Delta U = \Delta Q - \Delta W. \quad (4.1)$$

The work done can be mechanical (W_M),

$$W_M = P\Delta V + V\Delta P, \quad (4.2)$$

and/or electrical (W_e),

$$W_e = -nF\Delta E, \quad (4.3)$$

where n is the number of transferred charges, F is the Faraday constant equal to 96,485 C/mol, and ΔE is the maximum

potential difference due to the motion of charges. In other words, this is a statement of *conservation of energy*.

4.3.1.1 Enthalpy

The sum of the internal energy U and the work done by the reacting molecules to push the surroundings away, that is, to increase the volume of the system at constant pressure, is called *enthalpy* (H), expressed by

$$\Delta H = \Delta U + P\Delta V. \quad (4.4)$$

The change of enthalpy also gives the heat of reactions in chemistry. It is also calculated as the sum of the energies required to break old bonds minus the energies released from the formation of new bonds. The change in enthalpy is negative ($\Delta H < 0$) if the reaction is exothermic and positive ($\Delta H > 0$) if the reaction is endothermic. In the case of constant pressure, the change in enthalpy is simply equal to the heat added to the system (Q).

4.3.1.2 Entropy

Entropy (S) is most commonly described as a measure of the order in a system. Ordered systems have low entropy because the probability that a system is in an ordered state is low. When heat is added to the system it causes particles to move faster, and if the temperature is high enough bonds will be broken and the new state will be less ordered than before. Consider, for example, melting ice. The amount by which entropy has increased is given by

$$\Delta S = \frac{\Delta Q}{T}. \quad (4.5)$$

4.3.2 The Second Law of Thermodynamics

The second law of thermodynamics states that if a system is isolated (no energy is added to it), its entropy will only increase with time. Consider a plant that has been cut and left without water in a closed container. The plant will eventually decay, that is, its entropy has increased. Life requires input of energy to sustain order. Such processes are called *endergonic*. The energy of the final state is higher than the energy of the initial state.

4.3.2.1 Gibbs Free Energy

Gibbs free energy (G) is the energy that determines whether a reaction will be spontaneous or not. It is defined as the change in enthalpy minus the temperature times the entropy, shown in Equation 4.6:

$$\Delta G = \Delta H - T\Delta S = \Delta U + P\Delta V - T\Delta S. \quad (4.6)$$

The free energy for unfavorable (not spontaneous) reactions is positive ($G > 0$). Reactions will be spontaneous if the free energy is negative ($G < 0$). These reactions are classified as endergonic and exergonic, respectively.

During redox reactions, the Gibbs free energy is equal to the maximum electric work:

$$\Delta G^{\circ} = -nF\Delta E^{\circ}, \quad (4.7)$$

where the superscript "o" indicates standard conditions (25°C temperature and 1 atm pressure) and ΔE is the electric potential. It can be shown that at any temperature, Equation 4.8 represents the energy balance:

$$\Delta G = \Delta G^{\circ} + RT \ln Q_r, \quad (4.8)$$

where R is the gas constant ($R = 8.314$ J mol^{-1} K^{-1}) and Q_r is the reaction quotient.

As a result of the difference in ionic concentrations in the intra- versus extracellular space in biological cells, a potential difference is generated that can be calculated by combining the previous two equations in the following way:

$$-nF\Delta E = -nF\Delta E^{\circ} + RT \ln Q_r. \quad (4.9)$$

The result is called the Nernst equation, which is also referred to as the Nernst potential:

$$\Delta E = \Delta E^{\circ} - \frac{RT}{nF} \ln Q_r. \quad (4.10)$$

Therefore, Equation 4.10 gives the potential difference generated in a galvanic cell as a function of the ion concentrations in both compartments. This is called the *resting potential* during equilibrium. In this equation, Q_r represents the ratio of the extracellular to intracellular concentrations. This equation only represents a simple case in which the membrane is only permeable to one type of ion (e.g., only K^+ ions).[2] A more realistic expression for Q_r will be given later.

Cells are surrounded by membranes, which control the flow of ions in and out of the cell by the use of voltage gated ion channels and gap junctions.

4.4 Ion Channels and Gap Junctions

It has been found that there are passages, called *gap junctions*, connecting cardiac cells that are insulated from extracellular space and are wide (with a diameter of about 16 Å).[3] These channels have a very low resistance and are considered to have fixed anions that will select incoming ions based on their electronegativity and size. The other type of structure that is responsible for the flow of charges in the cell is called *ion channels*. These channels are gates that can transmit certain ions or molecules when activated by changes in the potential difference across the membrane or activated by extracellular or intracellular transport molecules (also called ligands) that attach to it.

The membrane potential depends directly on the concentrations of the ions on both sides. For example, let us assume that only K^+, Na^+, and Cl^- are allowed to flow through the membrane.

The expression for the membrane resting potential can be derived from the Nernst equation (Equation 1.10).[4] The resultant equation is also called the Goldman voltage equation, given by[2]

$$V_m = \frac{RT}{F} \ln \frac{P_{Na}[Na^+]_{out} + P_K[K^+]_{out} + P_{Cl}[Cl^-]_{in}}{P_{Na}[Na^+]_{in} + P_K[K^+]_{in} + P_{Cl}[Cl^-]_{out}}. \quad (4.11)$$

In this equation $P[Na^+]$ is the permeability constant for the Na^+ ion. A typical value for the resting potential is −90 mV.[5] It is negative because cells are more negative relative to the surrounding medium. Cells that are excitable have the ability to rapidly reverse the potential, causing it to be slightly positive. The potential that is generated in this process is known as the *action potential*.

4.5 Action Potential

The resting state of a membrane is the one in which the inside is more negative than the outside. As mentioned in the above section, a typical value is about −90 mV. Excitation from other parts of the membrane can trigger the opening of the sodium ion channels, which will cause Na^+ ions to flow into the cell. As a result the membrane potential will become more positive. This process is called *depolarization*. Once the potential reaches a certain *threshold* value (Figure 4.1), more sodium channels start opening very fast. This corresponds to the part of the potential curve on the picture where the rise of the potential is very steep. The total change in the potential is around 100 mV. When the potential reaches its maximum value, a number of Na^+ channels will begin to close and K^+ channels will open. The potential starts falling back toward its original value—repolarization. It will fall slightly below the resting value (*hyperpolarization*) but it will recover. This is, in short, a description of the action potential in a neuron. It is very similar to the one in a heart muscle cell, except that the action potential of a ventricular myocyte lasts longer and has a "plateau" area in which the potential stabilizes for a short period of time. This is due to the balance between the Ca^{2+} current flowing into the cell and the K^+ current flowing out (Figure 4.3).

4.6 Models of Ionic Current

After performing their famous experiments on a giant *nerve* fiber, A. L. Hodgkin and A. F. Huxley modeled their results comparing the cell membrane as a simple circuit in which there are three conductive elements (ion channels) connected in parallel (Figure 4.2).[6] Sodium, potassium, and "leakage" currents flow through each one of these. The conductance of each channel varies with time, as observed during the experiments, but the potential difference (E_{Na}, E_K, and E_L) for each one stays the same. The ionic currents are expressed in terms of the sodium, potassium, and leakage conductances, as shown by Equation 4.12:

$$\begin{aligned} I_{Na} &= g_{Na}(V - V_{Na}), \\ I_K &= g_K(V - V_K), \\ I_L &= g_l(V - V_L), \end{aligned} \tag{4.12}$$

where V_{Na}, V_K, and V_L are the differences between the resting potential and the equilibrium potential for each ion. V is the difference between the measured value of the potential and the absolute value of the resting potential. As previously mentioned,

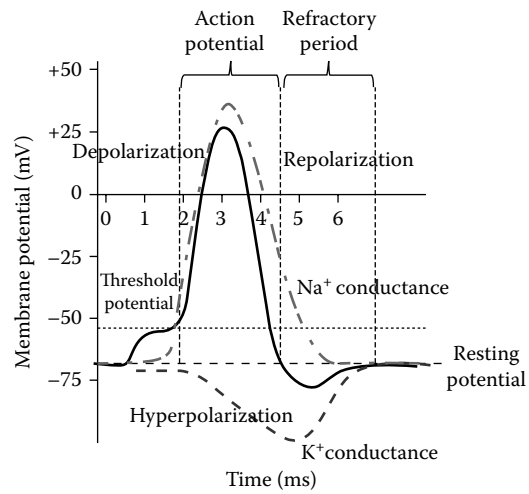

FIGURE 4.1 Action potential of a ventricular myocyte. Action potential on a 100 μm × 100 μm × cardiac tissue.

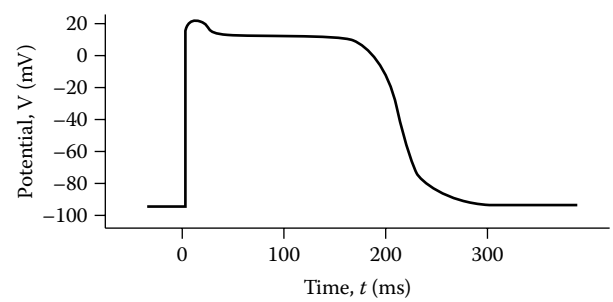

FIGURE 4.2 Action potential of an excitable cell.

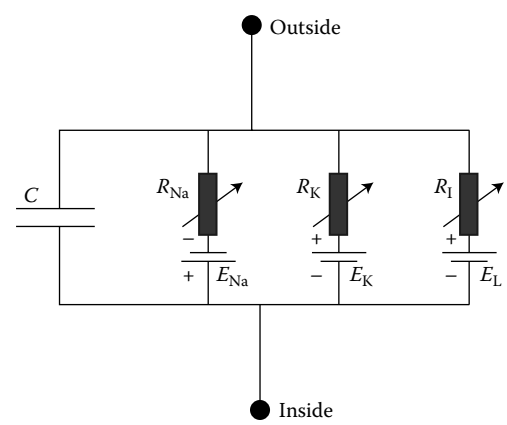

FIGURE 4.3 Circuit model of a squid axon membrane. (Modified from Hodgkin, A. L. and A. F. Huxley, *Journal of Physiology* 117: 500–544, 1952.)

the conductances are functions of both time and voltage. The *conductance of the potassium* ions was modeled by Hodgkin and Huxley, as represented by Equations 4.13 and 4.14:

$$g_K = \bar{g}_K n^4, \tag{4.13}$$

$$\frac{dn}{dt} = \alpha_n(1-n) - \beta_n n, \tag{4.14}$$

where $\bar{g}_K$ is a constant that is equal to the maximum value of g_K and has units of conductance/cm^2 and n is a dimensionless variable that can only take values from 0 to 1. The latter has been described as the "portion of particles in a certain position (e.g., at the inside of the membrane) and $1 - n$ represents the portion that is somewhere else."[6] This parameter has also been described in the literature as the activation parameter representing the ion channels. It represents the probability of the channels being open if there are a large number of channels.[2] The coefficients α_n and β_n are the rates of ion transfer in both directions: from outside and from inside, respectively. They vary with voltage but not with time and have units of [time]$^{-1}$. The functions α_n and β_n were obtained by fitting the experimental data for n, as shown in Equations 4.15 and 4.16:

$$\alpha_n = 0.01\frac{(V+10)}{\left[\exp\left((V+10)/10\right)-1\right]}, \tag{4.15}$$

$$\beta_n = 0.125\exp\left(\frac{V}{10}\right). \tag{4.16}$$

The *sodium* (Na) *conductance* is modeled in a similar way, Equations 4.17 through 4.19:

$$g_{Na} = m^3 h \bar{g}_{Na}, \tag{4.17}$$

$$\frac{dm}{dt} = \alpha_m(1-m) - \beta_m m, \tag{4.18}$$

$$\frac{dh}{dt} = \alpha_h(1-h) - \beta_h h, \tag{4.19}$$

where m represents the proportion of activating molecules inside the cell, h is the proportion of inactivating molecules on the outside, α_m and β_m are the transfer rates for the activating molecules inside the cell, and α_h and β_h are the same rates for the inactivating molecules. The equations that best fit the data are expressed by Equations 4.20 through 4.23[6]:

$$\alpha_m = 0.1\frac{(V+25)}{\left[\exp\left((V+25)/10\right)-1\right]}, \tag{4.20}$$

$$\beta_m = 4\exp\left(\frac{V}{18}\right), \tag{4.21}$$

$$\alpha_h = 0.07\exp\left(\frac{V}{20}\right), \tag{4.22}$$

$$\beta_h = \frac{1}{\left[\exp\left((V+30)/10\right)+1\right]}. \tag{4.23}$$

Therefore, the total ionic current can be expressed as the sum of all the ionic currents shown by Equation 4.24:

$$\begin{aligned} I &= I_K + I_{Na} + I_L, \\ I &= C_M\frac{dV}{dt} + \bar{g}_K n^4(V - V_K) + \bar{g}_{Na} m^3 h(V - V_{Na}) \\ &\quad + \bar{g}_L(V - V_L). \end{aligned} \tag{4.24}$$

Other models of the action potential include the same type of differential equations but introduced different formulations of the ionic current. The action potential of heart tissue is more complex than that for nerve fibers. That requires the equations and parameters to be adjusted in order to reflect those differences. For example, G. Beeler and H. Reuter modeled the action potential for *mammalian ventricular cardiac* muscles by representing the potassium current as composed of both time-independent outward potassium current, I_{K1}, and time- and voltage-dependent component, I_{Kx}. The first is also called the "outward rectification" current, and the latter is the inward rectification current.[7] In other words,

$$I = I_{K1} + I_{Kx} + I_{Na} + I_{Ca} - I_S. \tag{4.25}$$

Here I_S is the slow current flowing into the cell that is mainly carried by calcium ions.

Other, more recent models include even more detailed descriptions of the current. When describing action potentials and pacemaker activity, DiFrancesco and Noble suggested that in addition to the currents mentioned above, the total current includes the hyperpolarizing-activated current I_f, the transient outward current I_{to}, the background sodium and calcium currents $I_{b,Na}$ and $I_{b,Ca}$, the Na–K exchange pump current I_p, the Na–Ca exchange current I_{NaCa}, and the second inward current I_{si} given by Equation 4.26[8]:

$$\begin{aligned} I_{tot} &= I_f + I_K + I_{K1} + I_{to} + I_{b,Na} + I_{b,Ca} + I_p \\ &\quad + I_{NaCa} + I_{Na} + I_{Ca,f} + I_{Ca,s} + I_{pulse}. \end{aligned} \tag{4.26}$$

As more experimental data on the ionic currents became available, the mathematical models became more sophisticated in order to achieve higher accuracy in describing *human atrial* currents. Courtemanche et al.[9] described the membrane currents using the formulations of Luo and Rudy,[10] but adjusting the values for the parameters to fit the action potential for human atrial cells. Their model describes well the variations in Ca^{2+}, Na^+, and K^+ ion concentrations inside the cell by also including pumps and exchangers. The extracellular concentrations of ions are considered fixed. The total current according to their model is given by

$$\begin{aligned} I_{tot} &= I_{Na} + I_{K1} + I_{to} + I_{Kur} + I_{kr} + I_{ks} + I_{Ca,L} + I_{p,Ca} \\ &\quad + I_{NaK} + I_{NaCa} + I_{b,Na} + I_{b,Ca}. \end{aligned} \tag{4.27}$$

In this equation I_{Kur} is the ultrarapid delayed rectifier K^+ current, I_{kr} is the rapid delayed rectifier K^+ current, and I_{Ks} is the slow delayed rectifier K^+ current. The model handles the Ca^{2+} ion exchange by representing three calcium ion currents: $I_{Ca,L}$—L-type inward Ca^{2+} current, $I_{p,Ca}$—sarcoplasmic Ca^{2+} pump current, $I_{b,Ca}$—background Ca^{2+} current, and I_{NaCa}—Na^+/Ca^{2+} exchange current. Some of the current descriptions are given below.

As in the Luo–Rudy model the expression for the sodium current has an additional parameter, *j*, called the slow inactivation parameter, as shown in Equation 4.28:

$$I_{Na} = g_{Na} m^3 hj(V - V_{Na}). \tag{4.28}$$

The maximum sodium conductance was temperature adjusted ($g_{Na} = 7.8$ nS/pF) to reflect experimental data and also to produce the correct amplitude for the action potential. The expression for the I_{K1} current that best represents current and resistance measurements is given in Equation 4.29 (assuming no temperature dependence):

$$I_{K1} = \frac{g_{K1}(V - V_K)}{1 + \exp[0.07(V + 80)]}. \tag{4.29}$$

Here, the value for g_{K1} was set to be 0.09 nS/pF. The transient outward and ultrarapid are represented in a similar way. The gates o_a and u_a are the activation gates for I_{to} and I_{Kur}, respectively, and o_i and u_i are their inactivation gates, expressed by Equation 4.30:

$$\begin{aligned} I_{to} &= g_{to} o_a^3 o_i (V - E_K), \\ I_{Kur} &= g_{Kur} u_a^3 u_i (V - E_K), \\ g_{Kur} &= 0.005 + \frac{0.05}{1 + \exp\left[(V - 15)/-13\right]}. \end{aligned} \tag{4.30}$$

The descriptions of the rest of the currents are given in great detail by the author.[9] The flow of ions across the cell membrane is governed by the Nernst–Planck diffusion equation (Equation 4.31), in which the flux of ions J_K (current/area) is calculated as a function of the concentration of the species of interest C_K and the diffusion constant D_K[11]:

$$\vec{J}_K = -D_K\left(\vec{\nabla} C_K + \frac{C_K}{\alpha_K}\vec{\nabla} V\right), \tag{4.31}$$

where V is the potential due to the electric charge distribution and $\alpha_K = RT/FZ_K$ with Z_K the valence of the ionic species, R the gas constant, F the Faraday constant, and T the absolute temperature.

The diffusion equation can be solved numerically by implementing the Crank–Nicholson scheme expressed by Equation 4.32[12]:

$$\frac{1}{r_a}\left(\frac{\partial^2 V}{\partial x^2} + \frac{\partial^2 V}{\partial y^2} + \frac{\partial^2 V}{\partial z^2}\right) = C_m \frac{\partial V}{\partial t} + I_{Na} + I_{Ca} + I_K + I_{stim}, \tag{4.32}$$

where r_a is the resistance of the intracellular medium, C_m is the capacitance of the cell membrane, I_{stim} is the stimulation current, and I_{Na}, I_{Ca}, and I_K are the sodium, calcium, and potassium currents, respectively. Let V_m^n represent the voltage of the *m*th spatial element on the grid at the *n*th iteration (point in time). The second partial derivatives can be rewritten as

$$\frac{\partial^2 V}{\partial x^2} = \frac{1}{2h_x^2}\left[\left(V_{m+1}^{n+1} - 2V_m^{n+1} + V_{m-1}^{n+1}\right) + \left(V_{m+1}^n - 2V_m^n + V_{m-1}^n\right)\right], \tag{4.33}$$

where h_x is the spatial interval along the *x*-axis. Another approximation has been made for the current as follows:

$$I_m^{n+1} = I_m^n + \frac{dI_m^n}{dV}\left(V^{n+1} - V^n\right) + \cdots. \tag{4.34}$$

After rearranging some terms the diffusion can be factorized, which will help simplify the solution, as shown by Equation 4.35.

$$\frac{1}{(2 + k\Delta t)^2}(2 + k\Delta t - \Delta t\alpha_x)(2 + k\Delta t - \Delta t\alpha_y)(2 + k\Delta t - \Delta t\alpha_z) = 2\Delta t\left(\alpha(V)^n - \frac{I_m^n}{C_m}\right), \tag{4.35}$$

where

$$\alpha(V) = \frac{1}{r_a}\left(\frac{\partial^2 V}{\partial x^2} + \frac{\partial^2 V}{\partial y^2} + \frac{\partial^2 V}{\partial z^2}\right), \tag{4.36}$$

$$\alpha_i^n = \frac{1}{h_i}\left(\frac{V_{i+1}^n - V_i^n}{h_i R_{i2}} - \frac{V_i^n - V_{i-1}^n}{h_i R_{i1}}\right), \tag{4.37}$$

$$k = \frac{1}{C_m}\frac{dI_m^n}{dV}. \tag{4.38}$$

In these relations $i = x$, y, or z and h_i is the spatial interval along the *x*-, *y*-, or *z*-axis.

A representative solution to Equations 4.35 through 4.38 for select parameters are presented in Figure 4.4.

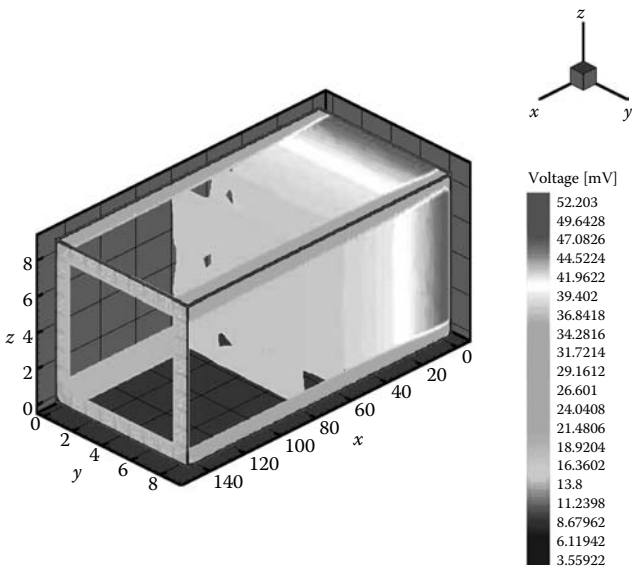

FIGURE 4.4 Numerical solution to Equation 4.35 for a 100 μm × 100 μm × 100 μm dimensional slab of cardiac tissue. Gap junctions have been represented as randomly distributed resistances in the tissue. Parameters used to generate this result are the following: membrane capacitance 6.28 nF/cm; cytoplasmic resistance 79.5 MΩ/cm; gap junction resistance 397.8 MΩ/cm; maximum sodium conductance 15 mS/cm^2; maximum calcium conductance 0.09 mS/cm^2; stimulation current −150 μA/cm^2.[11–14]

References

1. Physikalisch-Meteorologisches Observatorium Davos/World Radiation Center. 29 Feb. 2008. 10 Apr. 2009; http://www.pmodwrc.ch/
2. Fain, G. L., *Molecular and Cellular Physiology of Neurons*. Cambridge: Harvard, 1999.
3. Zipes, D. P. and M. D. Jose Jalife, Physiology of cardiac gap junction channels. In *Cardiac Electrophysiology*, pp. 62–69. Philadelphia: Saunders, 1990.
4. Hille, B., Ionic selectivity of Na and K channels of nerve membranes. *Membranes* 3: 255–323, 1975.
5. Klabunde, R. E., *Cardiovascular Physiology Concepts*. N.p.: Lippincott, 2004.
6. Hodgkin, A. L. and A. F. Huxley, A quantitative description of membrane current and its application to conduction and excitation in nerve. *Journal of Physiology* 117: 500–544, 1952.
7. Beeler, G. W. and H. Reuter, Reconstruction of the action potential of ventricular myocardial fibers. *Journal of Physiology* 268: 177–210, 1977.
8. DiFrancesco, D. and D. Noble, A model of cardiac electrical activity incorporating ionic pumps and concentration charges. *Philosophical Transactions of the Royal Society of London*. Series B. 307: 353–398, 1985.
9. Courtemanche, M., R. J. Ramirez, and S. Nattel, Ionic mechanisms underlying human atrial action potential properties: Insights from a mathematical model. *Am. J. Physiol. Heart Circ. Physiol.* 275.1: H301–H321, 1998.
10. Luo, C. and Y. Rudy, A model of the ventricular cardiac action potential. *Circulation Research* 68: 1501–1526, 1991.
11. Jack, J. J., D. Noble, and R. W. Tsien, *Electric Current Flow in Excitable Cells*. N.p.: Oxford, 1983.
12. Jacquemet, V. Steady-state solutions in mathematical models of atrial cell electrophysiology and their stability. *Mathematical Biosciences* 208.1: 241–269, 2007.
13. Pergola, N. F., Computer modeling of cardiac electrical activity: Methods for microscopic simulations with subcellular resolution. MS thesis. University of Tennessee, 1994.
14. Buchanan, J. W., et al., A method for measurement of internal longitudinal resistance in papillary muscle. *American Journal of Physiology* 251: H210–H217, 1986.

5

Action Potential Transmission and Volume Conduction

Robert Splinter

5.1 Introduction

The generation of the action potential is described in detail in Chapter 3. The depolarization potential has specific values for specific cell types and is always positive: +30 to +60 mV. The rising potential difference initially causes an avalanche effect due to the influence of the increasing potential on the sodium influx, which is self-maintaining. This process continues until the limit has been reached, after which the cell will actively repolarize the membrane potential locally. Meanwhile this depolarization has initiated the same depolarization process in the neighboring section of the cell, causing the depolarization front to migrate along the cell membrane until its physical end. In principle, the polarization front will obey the telegraph equation since the entire length of the membrane is supposed to follow the repetitive pattern outlined in Section 3.5.

Certain cells that have a different mechanism of propagation of the depolarization wave can be recognized. For instance, the action potential propagates along the length of the axon and dendrites of a myelinated nerve cell differently compared to the unmyelinated nerve cell.

Neurons are cells that specialize in the transfer of information within the nervous system. Neurons are excitable structures that are capable of conducting impulses across long distances in the body. They communicate with other cells by secretion of chemicals (neurotransmitter) to induce an action potential in the neighboring cell structure (e.g., the brain). When depolarization passes down a nerve fiber, there is exchange of ions across the membrane, resulting in changes in membrane potential at each point of the axon. The conduction process of an action potential can be compared to the movement of people in a stadium during a "wave." The motion of one person is induced by its direct neighbor; however, no physical longitudinal transportation of mass takes place. The process of "the wave" is illustrated in Figure 5.1. This is physically different from signal transmission in an electrical cord, where ions are passed through the cord and not exchanged with the environment outside it.

5.2 Components of the Neuron

The general structure of the nerve cell is outlined in Figure 5.2. The description of the nerve is as follows: cell body (perikaryon = around nucleus); single cell with receiving and transmitting lines: dendrites and axons, respectively. The cell body creates the transmitter molecules (neurotransmitter) for communication with neighboring cells at the synapse at the distal end of the axon. The dendrites are specialized features that receive information from other neurons (conduct the receptor signal to the cell body), and the axon is the cell extremity that has voltage gated channels to facilitate the creation and propagation of an action potential. Axons can be unmyelinated or myelinated. Myelin insulates the nerve cell, creating a leap-frog transmission instead of a cascading depolarization (Figure 5.3). Myelinated nerves have a significantly increased speed of conduction of action potentials compared to unmyelinated axons.

FIGURE 5.1 "The wave" performed by employees of The Spectranetics Corporation and students from UCCS in Colorado Springs, CO. No mass is moving; however, energy is transported from right to left in this picture as neighbors move upwards based on the incentive of the person to the left of each individual (for the viewer: right) as the wave moves to the left on the page. This process is very similar to the migration of turning dipoles on the cell membrane. The figure illustrates a monophasic transfer of potential energy from left to right, which will be described later in this chapter.

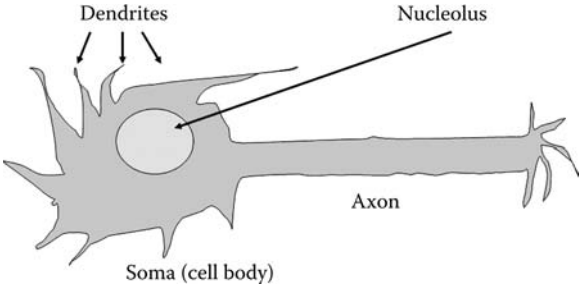

FIGURE 5.2 Schematic description of the construction of a nerve cell.

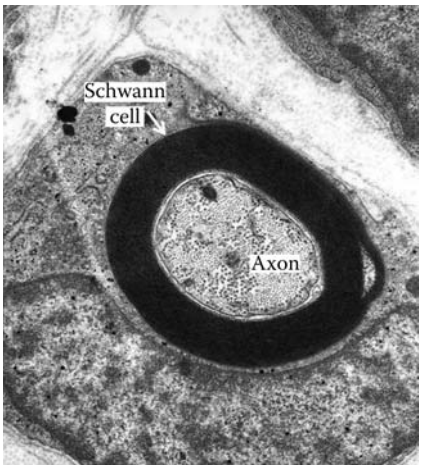

FIGURE 5.3 Electron microscope image of a cross section of a myelinated nerve cell with Schwann cells wrapped around the axon. (Reprinted from CRC-Press: Biomedical Signal and Image Processing, Taylor and Francis Press, 2006. With permission.)

5.3 Operation of a Nerve Cell

Stimulation of the nerve membrane can open ion channels in the membrane. Then Na^+ ions flowing in will depolarize the membrane (movement from −70 mV to say −60 mV) and K^+ ions flowing out of the membrane will hyperpolarize the membrane (−70 mV to say −90 mV). The spike at one point on an axon causes the adjacent neural membrane to change its permeability so that just beside the area where the spike just took place sodium rushes in and potassium rushes out, resulting in a spike there. This process repeats itself many times, resulting in the propagation of the action potential down the neuron. Since this moving spike is electrochemical rather than strictly electrical, it moves considerably more slowly than electricity in a wire. At body temperature, the depolarization and subsequent repolarization procedure lasts ~0.5 ms at one single point on the membrane.

5.3.1 Unmyelinated Nerve

The transmission of impulses in an unmyelinated membrane propagates as "the wave"; the lag time between the neighboring rise and fall (for the membrane: the transmembrane potential; in the audience: the standing and sitting response) is the refractory period. The refractory period is a function of the initiation of the chemical transfer, which is a voltage gated Na/K pump activation. The chemical migration of the Na and K ions is an active process and hence relatively slow. The propagation of the action potential is shown in Figure 5.4. The accompanying membrane potential gradient resulting from the action potential illustrated in Figure 4.1 is illustrated in Figure 5.5. The expression of the membrane potential at the surface of the body is described later on in this chapter.

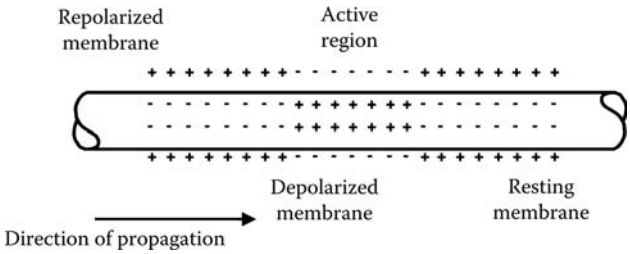

FIGURE 5.4 Schematic description of depolarization propagation in an unmyelinated axon.